Unity Mining Pty Ltd
Henty Gold Mine
ABN 61 005 674 073
Postal Address: PO Box 231 Queenstown TAS 7467
Site Office: Howards Road Queenstown TAS 7467
Phone: (03) 6473 2444
Facsimile: (03) 6473 1857

# EDGI ROUND 5

# HENTY PROJECT – 7M/1991

# DRILLING REPORT

# CEH001, CEH002, CEH003

# JUNE 2022

| | | | | |
|---|---|---|---|---|
| **HELD BY:** | UNITY MINING LTD | | | |
| **MANAGER & OPERATOR:** | Catalyst Metals Ltd | | | |
| **AUTHOR:** | P. Dale, R. Reid | | | |
| **DATE:** | June 2022 | | | |
| **MAP SHEETS:** | 1:25k | Dundas (3636) | Oceana | 3635 |
| | | Selina (3836) | Tyndall | 3835 |
| | 1:100k | Sophia | | |
| **GEOGRAPHIC COORDS (GDA94):** | Min East: | 378,111mE | | |
| | Max East: | 381,111mE | | |
| | Min North: | 5,358,934mN | | |
| | Max North: | 5,368,183mN | | |
| **COMMODITY(s):** | Au, Base metals | | | |

## Document Purpose

This report and attached files relating to drilling of CEH001 and 2, is provided to fulfil the requirements of the Final EDGI report, as detailed in section 9.3 of the "*EDGI Program **2018** – Guidelines for Project Proposal Submission"* document ("the Guidelines").

The combined direct drilling costs for CEH001, 002 and 003 $368,168. Under the Guidelines Catalyst Metals Ltd. is requesting payment of $50,000, being the unclaimed half of the total co-funded drilling amount ($100,000).

## Summary

Catalyst Metals Ltd (CML) was granted approval via its subsidiary Henty Gold Pty Ltd, for co-funded drilling north of the Henty Gold Mine under the Exploration Drilling Grant Initiative ("EDGI") Round 5. The Henty Gold Mine is located on the West Coast of Tasmania between Queenstown and Tullah, within ML7M/1991 (Figure 1).

The co-funded drilling grant for 50% of the direct drilling costs, up to $50,000, comprised three diamond drill holes (CEH001 255.5m EOH, CEH002 735m EOH, and CEH003 332.7m EOH) targeting potential northern extensions of the Sill Zone (Figure 2) and other features of geological significance.

A fence of five drillholes covering a 1,000m traverse was initially planned to establish stratigraphy around the Henty Fault and test for potential northern continuation of structurally controlled intrusion related gold mineralisation north of the Sill Zone (northern extent of the Henty orebody). The continuation of the Henty Fault has not been substantially tested due to perceived low prospectivity, which is based on a historic geological model that does not fit current available evidence. Ultimately, three holes were drilled totalling 1323.7m. Interpretation relating to collective results from Henty EDGI drilling is presented herein.

Drillholes were studied using conventional geochemistry, pXRF geochemistry, spectral analysis, magnetic susceptibility, and structural analysis. There were no significant economic findings in the three holes drilled. However, there is a zone of multi-element anomalism with sporadically elevated Au, Ag, As, Sb, Te, Hg, Cu, Pb & Zn associated with thin veins containing polymetallic sulphide mineralization. This zone is contained within a broad intense sericite-silica alteration zone within a high ductile strain structural zone, representing a probable post-Cambrian proto-shear and fluid pathway. Another zone of intense sericite alteration associated with a potentially Tabberaberan high strain zone in rhyolite in CEH002 is interpreted as a potential fluid pathway.

Lithochemical analysis indicates the volcanics and basalts of the CVC and Lower Tyndall are High K to shoshonitic calc-alkaline volcanics demonstrating a continuous broad evolution from basaltic through andesitic and dacitic to rhyolitic compositions. The study also found that the Henty volcanics are not prospective for porphyry style mineralization. Small variations in elemental abundance were used to discriminate inter and intra-lithological variation. Univariate wave tessellation analysis highlights major stratigraphic boundaries and potential lithological changes.

Further work is required to validate the interpretation of the identified zones and develop meaningful vectors for fluid source and pathway. This could involve additional drilling and exploration efforts to better understand the geology of the area and identify potential mineral deposits. The findings and conclusions of the report provide a solid foundation for further exploration of the area.

## Significant Findings

- No significant mineralisation was intersected in CEH002 although IRG style fluid pathways related to known mineralisation were identified. Vertical zonation in hydrothermal alteration and mineral styles at Henty indicate mineral emplacement post-basinal closure and likely within a window of favourable depth relative to paleosurface. It is interpreted that the favourable depth window has been uplifted and eroded away in the Henty North area, and that the area is not prospective for typical Henty style mineralisation.
    - Further work is required to validate the interpretation of Henty forming within a favourable depth window and until this theory is proven it remains possible there may be structural repetitions, dilations or suitable trap sites occurring at other depths resulting in further zones of mineralisation.
    - The depth window hypothesis also does not eliminate the potential for other styles and ages of mineralisation in the area, or major tectonic disruption downthrowing a block to the north and preserving the favourable depth window.
- In areas south of CEH002 (around and immediately north of the Sill Zone) it appears that folded sequences of Zig Zag Hill Formation, Mt Julia Formation and Owen Formation stratigraphies are oriented at a moderate angle to and terminating against the Henty Fault. Volcanic breccia of the Zig Zag Hill Formation is juxtaposed against the Henty Fault in CEH002, indicating that in this area dominant folding axes in these stratigraphies are oriented sub-parallel to the fault. The Zig Zag Hill Formation appears to overlie rhyolites of the Mt Julia Formation, indicating either that (a) folding proximal to the Henty Fault is still overturned, or (b) rhyolites intercepted may be an intruded part of the Suite 2 porphyry sequence rather than My Julia Rhyolite.
    - Apparent westward facing evolution of the rhyolite indicated by a general evolution towards more felsic composition with increasing Si, K & Al and decreasing Ti and Sr composition gives credence to the possibility that rhyolite intersected in the hole may be Suite 2 Porphyry rather than Mt Julia Formation. Sustained variations in iron content within the sequence indicate there are multiple rhyolite events within the mass. Further work would be required to assess this hypothesis.
- Relative palaeo-depth between Henty and the CEH002 intercept could not be established with confidence, however the CEH002 intercept is interpreted to be significantly deeper than the Henty Deposit, at an unfavourable depth for mineral precipitation and non-prospective.
- CEH002 intercepted a major brittle fault with a fault bound lithology to the east tentatively identified as Lower Tyndall Lynchford Tuff, which is a key stratigraphic marker horizon for Henty mineralisation. This unit is correlated with a similar intersection to the north in MX005, indicating potential presence of this prospective lithology over extensive distances north and east of Henty. Subject to other mineral controls such as depth, fluid pathways and structural complexity, this eastern repetition of the prospective stratigraphy presents a significant target opportunity.
- Both CEH001 & 002 intersected a significantly wider zone of cataclastic and broken faulting than holes along strike to north and south, indicating there is either a structural convergence

or divergence around this location. Oriented core was not able to be achieved in this heavily broken zone however no significant evidence of a converging structural attitude was observed so a divergence of the Henty Structure with an offshoot to the NNW is interpreted. The Henty Fault could not be identified on surface without earthworks so there are limited data points for correlation to establish fault attitudes. There is opportunity for localised structural dilations associated with the structural divergence.

- Lithochemical analysis of the lithologies between the eastern and western boundaries of the Henty Fault corridor (the Henty North and Henty South Faults respectively) indicates that these lithologies, originally logged as CVC, are Tyndall Group correlatives consistent with a rhyolitic or dacitic provenance. This indicates that the Henty Fault has progressed from west to east in its development with juxtaposition of the CVC (west) and Tyndall Group (east) temporally limited to early fault development (Henty South Fault event). It is observed in other drilling that the Henty South Fault (the western boundary fault) has locked up and healed in areas north of the target. We interpret that the eastern fault (Henty North Fault) is a more recent reactivation feature representing an eastern progression of the faulting activity.
- Drillhole CEH003 did not intercept any significant structure or mineralisation. The hole was targeting north-west oriented geochemical anomalism and interpreted structure. Due to environmentally limited scope to create drill sites, the hole was drilled targeting the southern extent of the geochemical anomalism. It is possible that mineralisation may develop further to the north-west, which can be tested with infill soil sampling.
- Lithological features were identified in folded CVC stratigraphy on the western side of the Henty Fault corridor which indicated potential for distal exhalative volcanogenic massive sulphide (VMS) mineral systems within that stratigraphy.
- The portable XRF instrument has proven to be an effective tool in both lithochemical and pathfinder elemental analysis and interpretation. A larger population of readings is required than conventional ICPMS analysis because of the point-sample nature of pXRF, however the results are broadly comparable and relative variances are correlable between the methods. A Jensen Cation plot was found to provide the best sensitivity for discriminating relatively unaltered lithologies using this data.
- Lithochemical data indicate that the volcanics and basalts of the CVC and Lower Tyndall are High K to shoshonitic calc-alkaline volcanics demonstrating a continuous broad evolution from basaltic through andesitic and dacitic to rhyolitic compositions. There is a Late High-Mg tholeiitic basalt identified in holes CEH002 & 003. Andesite identified in CEH002 may also be later than the surrounding volcanics. The Henty volcanics (both Lower Tyndall and CVC) are not prospective for porphyry style mineralisation.
- Analysis of key vein orientations identified three main distributions. The Devonian NNW to NW strike trend is mostly reflected by silica, quartz and sericite features. A relatively flat thrust related trend is reflected by silica, quartz, carbonate, pyrite, tan silica-carbonate and to a lesser extent albite, chlorite and sericite veins. ENE to NE striking vein sets is reflected by chlorite, silica, quartz and galena. Base metals species galena and chalcopyrite commonly align to the Henty Fault strike orientation (~20TN).

# Table of Contents

Document Purpose ..... 2
Summary ..... 2
Significant Findings ..... 3
List of Figures ..... 6
List of Tables ..... 9
1. Introduction ..... 10
1.1. EDGI Program Round 5 Proposal ..... 10
1.2. Location & Access ..... 11
2. Activities Completed ..... 11
2.1. Drilling ..... 11
2.2. Spectral Analysis ..... 13
2.3. Conventional Geochemistry ..... 14
2.4. pXRF Geochemistry ..... 14
2.5. Magnetic Susceptibility ..... 15
2.6. Structural Analysis ..... 15
2.7. Rehabilitation ..... 16
3. Results Achieved ..... 16
3.1. Drilling ..... 17
3.1.1. CEH001 ..... 17
3.1.2. CEH002 ..... 19
3.1.3. CEH003 ..... 21
3.1.4. Fluid Pathways ..... 21
3.1.5. Major Structural Features ..... 22
3.2. Geochemistry ..... 23
3.2.1. Lithochemistry ..... 23
3.2.1.1. Lithochemical Discrimination ..... 27
3.2.1.2. Intra-Lithology Discrimination ..... 31
3.2.2. Pathfinder Chemistry ..... 36
3.3. Magnetic Susceptibility ..... 39
3.4. Spectral Analysis ..... 40
3.5. Alteration Classification ..... 41
3.5.1. Alteration Indices ..... 42

3.5.1.1. Assessment of Alteration Indices (ICPMS data) ..... 44
3.5.1.2. Assessment of Alteration Indices (pXRF data) ..... 44
3.6. Structural Analysis ..... 47
3.6.1. Folded Features ..... 47
3.6.2. Planar Features ..... 48
3.6.3. Fault Features ..... 50
3.6.4. Vein Features ..... 54
4. Conclusions ..... 56
References ..... 58

## List of Figures

Figure 1: Location diagram for original planned holes under EDGI 5 proposal. 11
Figure 2: Location diagram for completed drillholes under EDGI 5 drill program 12
Figure 3: Estimation of drilling cost per metre per drillhole 13
Figure 4: Graph of drillhole pXRF analyses for Si(left graph) and Al (right graph) over time (x axis), coloured by drillhole (red = CEH002, orange = CEH002, green =CEH003) and calibrations (blue) (calibrations using a Si blank standard). 14
Figure 5: Prognostic Section for EDGI Round 5 Grant application. 16
Figure 6: CEH001 at 79.8m showing pepperitic textures in volcanic sandstone uphole of a possible fold hinge. 17
Figure 7: CEH001 vein paragenesis examples showing left (@ 130m) Devonian buck quartz vein (uphole) cuts quartz-carbonate-chlorite vein which overprints low core axis angle weakly banded silica-sericite vein with proximal pyrite selvedge which cross-cuts foliation; and right (@ 173.6m) foliation disrupting earlier carbonate-chlorite-pyrite-chalcopyrite vein. 17
Figure 8: CEH001 at 217.44m (top) and at 223.77m (bottom, plunging -10° towards 212°TN) showing Z-style parasitic folds with vergence to an anticline uphole. The fold plunge likely reflects Henty Fault related/proximal folding, as compared to the more regional Devonian 150° fold hinge plunge / strike trend. The carbonate vein show (top) is emplaced pre-folding, foliation and sericite development. 18
Figure 9: Photo of CEH002 at 532.1m showing cream to grey laminar banded, medium grained crystal rich volcaniclastic sandstone, coarsening downhole and with potential relict truncated crossbedding indicating uphole facing. 19
Figure 10: CEH002 at 352m showing coarse grained quartz-feldspar phyric massive coherent rhyolite lava. 20
Figure 11: CEH002 at 625.1m (top) and 630.2m (bottom) showing polymict lithic volcaniclastic interpreted as a correlative of the Lower Tyndall Lynchford Tuff. 20
Figure 12: Interpreted Mount Read Volcanics Stratigraphy 21
Figure 13: NNW (335°) facing oblique view of wireframe of the Henty Fault Zone (left) and plan view of Henty Fault Zone (right) including lateral extension at the Platter Zone, demonstrating NW oriented flexure in HFZ identified by EDGI drilling. 22

Figure 14: Comparison of select downhole chemistry for hole CEH003 contrasting results from pXRF (top row) and ICPMS (bottom row). 24
Figure 15: Rock classifications of ICPMS data for drillholes CEH001, CEH002 & CEH003. 25
Figure 16: Ti-Zr diagrams (using Hallberg 1984 format) for pXRF data sequentially presenting core logged as Volcanic epiclastic & breccia, Rhyolitic, Andesitic, Dacitic crystalline tuff & breccia, Dacitic epiclastic, Basaltic. 25
Figure 17: Volcanic rock classifications (using a modified Pearce 1996 format) for pXRF data sequentially presenting core logged as Volcanic epiclastic & breccia, Rhyolitic, Andesitic, Dacitic crystalline tuff & breccia, Dacitic epiclastic, Basaltic. 26
Figure 18: Probability plots for Nb & Y data 27
Figure 19: Alumina saturation diagram showing all holes using ICPMS data. 27
Figure 20: Tectonic classification of EDGI data sets demonstrates most of the core analysed is Arc calc-alkaline, though some basalt samples present as tholeiitic. ICPMS date on left, pXRF on right. 28
Figure 21: Jensen Cation Plots for discriminating lithologies. ICPMS data only. 29
Figure 22: Th-Co Discrimination Diagram for classifying altered volcanic arc rocks. ICPMS on left, pXRF on right. 29
Figure 23: Porphyry prospectivity plots for Henty volcanics 30
Figure 24: CEH002 downhole plots of key elements demonstrating evolution of rhyolitic facies towards the west (inclined hole drilled west to east). Downhole plots have been restricted to around the 80th percentile of data to highlight trends in mean distribution. 31
Figure 25: Downhole Wavelet Tessellations of select elements demonstrating major stratigraphic boundaries at 249m (Western Henty Fault) (Fe, Sr, Ti, K, Al and 305m (start of Mount Julia Rhyolite unit (Si, Al, K). 32
Figure 26: Downhole Wavelet Tessellation plots for Mg in Holes CEH001, 002 & 003 showing correlations between similar mafic units in CEH001 & 002 (pink units), and other dacitic lithologies. 33
Figure 27: X-Y plots demonstrating unique geochemistry of altered interval in CEH002 & 003 (ICPMS data). Highlighted samples represent an altered interval. 34
Figure 28: Downhole plots of anomalous chemistry in CEH002 & 003 (ICPMS data). Highlighted samples represent an altered interval. 34
Figure 29: Example of core from 260-262m in CEH003 demonstrating alteration associated with chemistry outlined in Figure 27 & Figure 28. Full altered interval extends from 250-293m. 35
Figure 30: Downhole plots of pathfinder elements for CEH002 using ICPMS data (top) and pXRF data (bottom). 38
Figure 31: Ternary analysis of pathfinder elements demonstrating a Au-Ag-As metal association in a small sub-population of samples. This was found to be the most reliable metal association with gold identified in samples from this drilling program. 39
Figure 32: Analysis of positive correlations of (left to right) S & Fe with As, and of Fe, Hg, Ag & Zn with S (ICPMS data). 39
Figure 33: Spectral analysis of CEH003 samples. Mica diagram coloured by mineral type (mica diagram; green = phengite, blue = muscovite-phengite), (chlorite diagram; pink = FeChl, orange = FeMgChl, green = MgChl, blue = MgFeChl). 40

Figure 34: Spectral analysis of CEH001 samples. Mica diagram coloured by mineral type (mica diagram; orange = muscovite), (chlorite diagram; pink = FeChl, orange = FeMgChl, green = MgChl, blue = MgFeChl). 41
Figure 35: Comparison of logged Vs spectrally defined alteration for CEH003. Logged dominant alteration (Mg plot) shows albite-silica (orange), sericite (light green) chlorite (dark green) and quartz (pink). 41
Figure 36: Various alteration discrimination plots for determining trends in alteration style and intensity 42
Figure 37: Select alteration characterisation plots for analysing trends in alteration 43
Figure 38: Downhole plots of CEH001, 002 & 003 for exploration indices ISER, AI, CCPI, MSI & ACNK using ICPMS data (all plots). X axis is consistent between each hole for each index. Y axis is presented at different scales to provide better data resolution. 45
Figure 39: Downhole plots of CEH001, 002 & 003 for MSI exploration index using ICPMS data (1st row) and pXRF data (2nd row). X-axis is consistent for all plots and the Y-axis is presented at same scale for all plots. 46
Figure 40: All fold hinges for folds, kink bands and veins in CEH001-003 displaying dominant ~20 to 175°TN plunge with a lesser population at 60 to 335°TN. 47
Figure 41: Folds defined by bedding and banding showing dominant ~30 to 195°TN axial plunge. 47
Figure 42: Folded vein axial plane plunge and trend. 48
Figure 43: Kink Bands in CEH002 48
Figure 44: Plot of all CEH poles to planes for beds and banding. 48
Figure 45: Poles to planes for all Contacts with respect to HFZ East and West domains. 49
Figure 46: Basalt Contacts (poles to planes). BVU = undifferentiated basalt, BASL = basalt lava, BASS= basaltic sandstone & BIN = basalt intrusive. 49
Figure 47: Plot of poles to foliation planes. 49
Figure 48: Stereoplot of poles and great circles to planes for **all structural features** identified in CEH001, 002 & 003. 50
Figure 49: Shear sense (poles to planes and Rose diagram) for all orientated fault features in the **WHFZ domain**. 51
Figure 50: Shear sense (poles to planes and Rose diagram) for all orientated fault features in the **EHFZ domain**. 51
Figure 51: Shear sense (poles to planes and Rose diagram) for all orientated **Dextral** fault features. 52
Figure 52: Shear sense (poles to planes and Rose diagram) for all orientated **Sinistral** fault features. 52
Figure 53: Shear sense (poles to planes and Rose diagram) for all orientated **Reverse** fault features. 53
Figure 54: Shear sense (poles to planes and Rose diagram) for all orientated **Normal** fault features. 53
Figure 55: Gridded density for all oriented veins (poles to planes). 54
Figure 56: Gridded density for all oriented dominant vein mineral specie (poles to planes) illustrating key vein orientations. 54
Figure 57: Gridded density for all oriented veins by contained mineral specie (poles to planes) regardless of vein proportion. 55

## List of Tables

Table 1: EDGI Round 5 drillhole collar details ..... 12
Table 2: Detailed breakdown of drilling costs for EDGI Round 5 drilling program ..... 12
Table 3: Activities completed in processing drill cores. ..... 13
Table 4: Elemental range and detection limits for conventional ICPMS geochemistry. ..... 14
Table 5: Elemental range and capabilities of the Vanta-M pXRF instrument. ..... 15
Table 6: Legend for all geochemical data presented in this report. ..... 23

# 1. Introduction

## 1.1. EDGI Program Round 5 Proposal

The North Henty area had been downgraded by previous operators because the limited knowledge of the area did not meet the conditions for the historically preferred stratiform controlled mineralisation model. Further, the economic gold mineralisation on the Henty Mine corridor was thought to terminate at its intersection with a cross-cutting massive rhyolite. No work had been conducted to investigate the nature and impact of this rhyolite beyond its intersection with the known mineralised zone.

Catalyst's initial review of the North Henty area found that the region had not been adequately or effectively explored. There were only five intercepts of the Henty Fault over a strike length of 3,500m, averaging one intercept per 700m of strike. These holes on average provided only a 60m intersection of the prospective footwall structural position east of the Henty Fault, which is the equivalent structural position of the Henty Mine mineralisation.

Catalyst found that there is evidence of continuity of magmatic style (IRG) mineralisation north of the rhyolite sill that terminates the Henty ore. A mineral systems model is being developed using evidence from within the mine and from historic exploration. This model suggests several preconditions for economic mineralisation including structural and alteration preparation that have contributed to triggering gold precipitation in a relatively younger (possibly Tabberaberan) event than suggested in previous models.

The ongoing program will test and further develop the new exploration model for Henty style mineralisation and will contribute to planning of a second stage of drilling to assess the poorly tested strike extent of the Henty Fault, as well as any additional prospective structures / positions that may be identified or deduced.

## 1.2. Location & Access

ML7M/1991 is centred approximately 23.5 km north of Queenstown in western Tasmania (Figure 1).

Access to ML7M/1991 area from the south is via the Anthony Road (B28), the unsealed Howards Road to the Henty mine site, then by mine service roads and formed 4WD tracks.

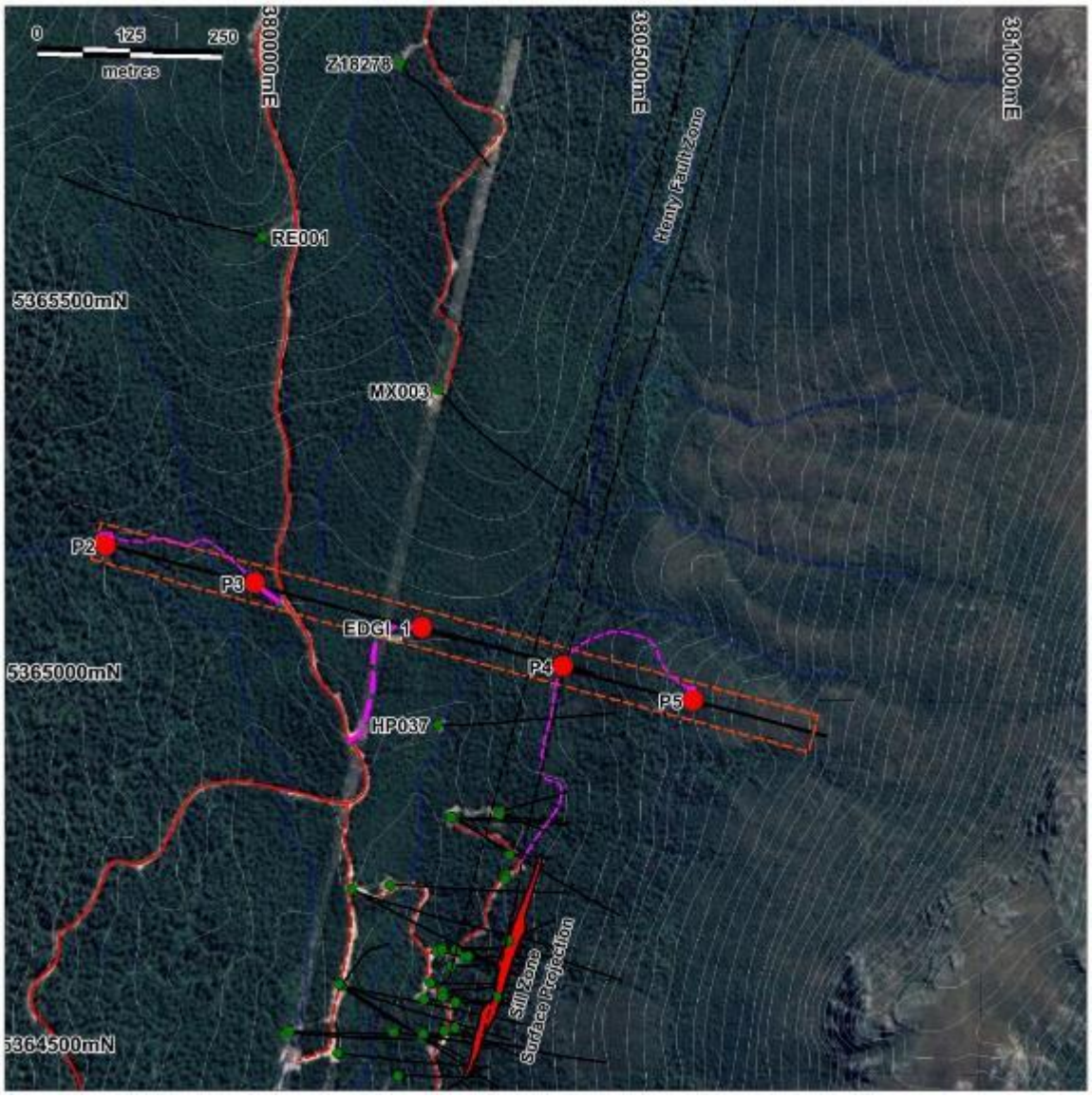


*Figure 1: Location diagram for original planned holes under EDGI 5 proposal.*

# 2. Activities Completed

## 2.1. Drilling

Drilling of CEH series holes was undertaken by Edrill Pty. Ltd. using a CS1000 P4 diamond drill rig. The program commenced in late August 2021 under the supervision of Catalyst Exploration Superintendent Paul Dale and Consultant Geologist Robert Reid. Initially the rig operated single shift 5 days per week and progressed to double shift 5 days per week in December. The three holes reported here were completed in January 2022.

Drilling comprised a total of 1323.7m, including 530.2m HQ and 793m NQ diamond core. Full details of the hole coordinates, azimuth, inclination and drilling dates are shown in Figure 1 and appended digital data (see ML7M1991_202206_00_Filelisting.xlsx). All drilling, map and location data provided in the report use the GDA 94 (Zone 55) reference datum. Drill cores for holes CEH002 & CEH003 will be submitted to MRT's Mornington Core Library.

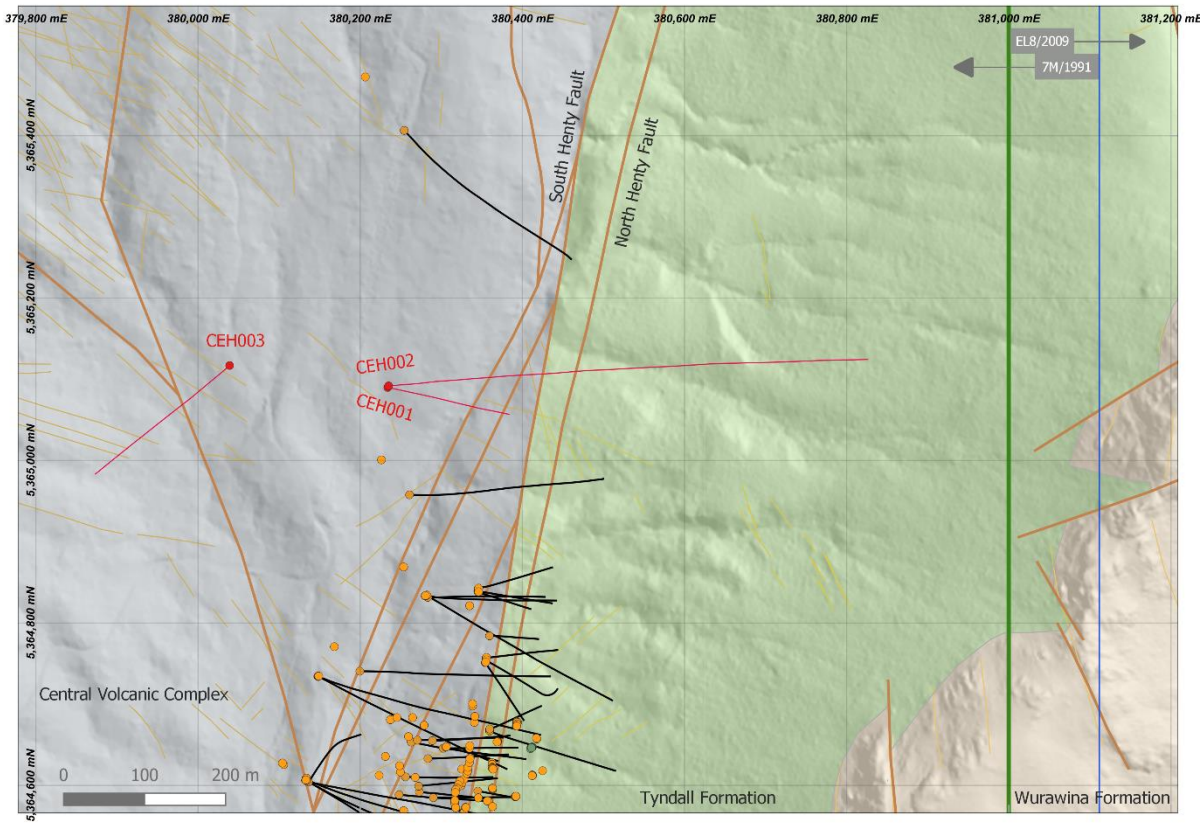


*Figure 2: Location diagram for completed drillholes under EDGI 5 drill program.*

| Hole ID | East GDA94 | North GDA94 | RL (mAHD) | Azimuth (TN) | Dip | End Depth |
|---|---|---|---|---|---|---|
| CEH001 | 380234.6 | 5,365,090.2 | 635.7 | 103.35 | -55 | 255.5 |
| CEH002 | 380233.6 | 5,365,089.0 | 635.7 | 89.00 | -50 | 735.0 |
| CEH003 | 380039.1 | 5,365,116.8 | 630.6 | 228.85 | -55 | 332.7 |

*Table 1: EDGI Round 5 drillhole collar details*

| Hole ID | HQ(m) | NQ(m) | HQ($) | NQ($) | Active($) | Inactive($) | Consum. | Total ($) |
|---|---|---|---|---|---|---|---|---|
| CEH001 | 119.6 | 135.9 | 16,842 | 17,567 | 39,900 | 14,560 | 10,531 | 99,400 |
| CEH002 | 320.7 | 414.3 | 46,870 | 71,283 | 31,850 | 8,120 | 30,279 | 188,406 |
| CEH003 | 89.9 | 242.8 | 12,586 | 32,215 | 21,350 | 5,880 | 8,330 | 80,362 |

*Table 2:* Detailed breakdown of drilling costs for EDGI Round 5 drilling program

The direct drilling cost for CEH001, 002 & 003 totals $368,168. This value is comprised of HQ and NQ drilling/metre costs, work time (running rods, casing holes, orientation surveys, etc) and drilling consumables/fluids. Details of breakdown of drilling costs are presented in (Table 2) and an estimation of downhole costs per metre are presented in (Figure 3). Significant mobilisation / demobilisation cost were also incurred for excavator hire, utilised for access track and drill pad preparation, as well as mobilising drilling gear to site, north of the Henty Gold Mine.

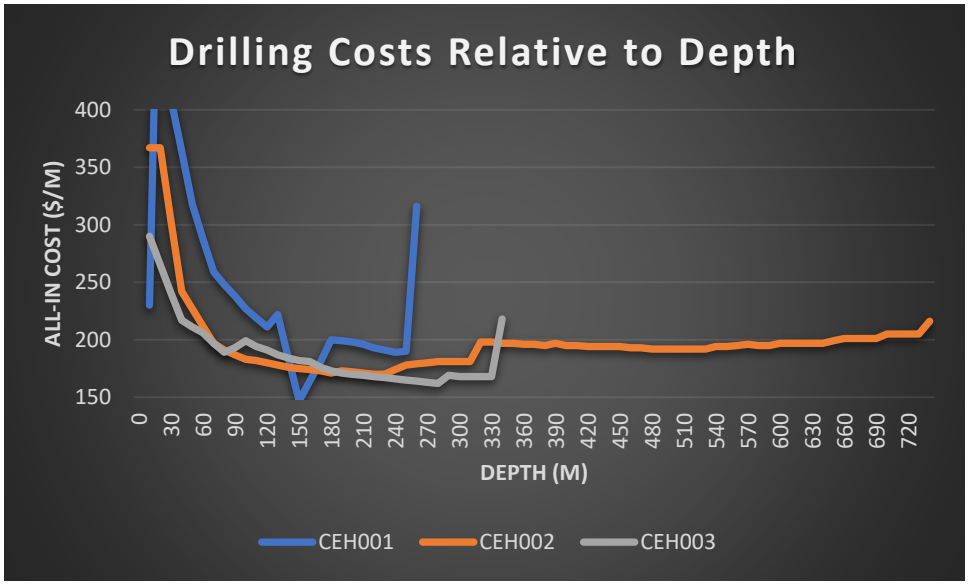


*Figure 3:* Estimation of drilling cost per metre per drillhole

Processing of drill core included activities described in Table 3 and in subsequent parts of Section 1 of this report.

| Activity | Number samples / metres processed | Details |
|---|---|---|
| Conventional geochemistry | 187 samples | ALS ME MS61L & Au-AAS25 |
| Spectral analysis | 187 samples | ALS TRSPEC 20 |
| pXRF geochemistry | 2,370 readings<br>61 readings | Lithochemistry & pathfinder analysis<br>QAQC |
| Magnetic susceptibility | 2,588 samples | CEH001 n=490, CEH002 n=1440, CEH003 n=658 |
| Core logging | 1,323.7m<br>(530.2m HQ / 793m NQ) | Geological, structural & geotech logging, core photography |

*Table 3: Activities completed in processing drill cores.*

## 2.2. Spectral Analysis

Sample pulps from holes CEH001 & 003 were submitted for TRSPEC hyperspectral analysis. Results have been reported but are not analysed here.

## 2.3. Conventional Geochemistry

A total of 187 conventional analytical samples were taken from CEH001 (n=34) and CEH003 (n=153). These were analysed by ALS using multi-acid digest followed by low level ICPMS determination of 48 elements (ME-MS61L), and 25g aliquot AAS determination of Au (Au-AA25).

| Limit of Detection | Elements Analysed |
|---|---|
| >1 ppm | Al, Ca, K, Mg, S - 0.01%; Fe – 0.002%; Ti, P - 0.001% |
| 1 ppm | Ba |
| 0.1-0.2 ppm | Cr, Li, Mn, V, Zn, Zr |
| 0.01-0.09 ppm | As, Be, Ce, Cs, Cu, Ga, Ge, Mo, Ni, Pb, Rb, Sb, Sc, Sn, Ta, U, Y |
| 0.002-0.009 ppm | Ag, Bi, Cd, Co, Hf, In, La, Se, Te, Th, Tl, W |
| <0.001 ppm | Au, Re, Na |

*Table 4:* Elemental range and detection limits for conventional ICPMS geochemistry.

## 2.4. pXRF Geochemistry

A total of 2,370 pXRF readings were collected at a variety of nominal intervals dependant on consistency of lithology and alteration. Readings are made directly onto round core. To maintain data population integrity, a minimum of two readings were taken within each unique unit (combined lith/alt). Readings were taken at nominally 3m intervals in extensive consistent lithologies, and progressively spacings are tightened to nominally 0.5m in variable units or areas of interest. Elements analysed and detection limits are described in Table 5.

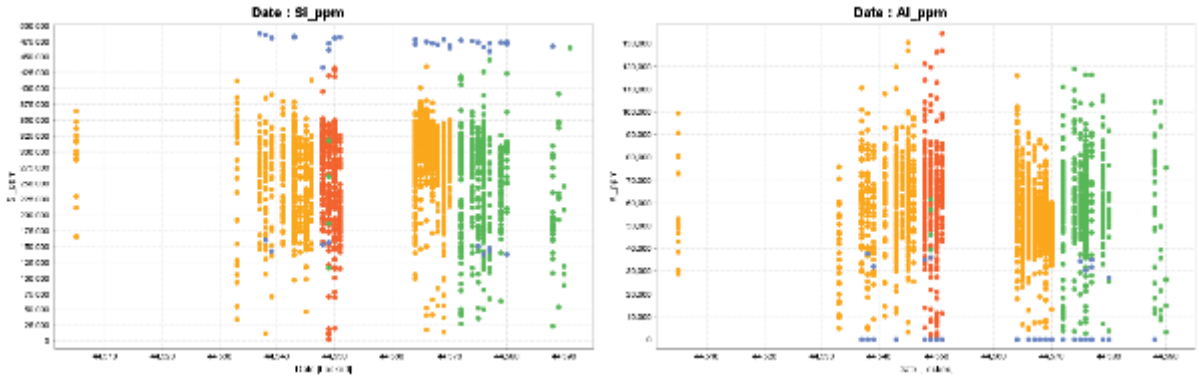


*Figure 4: Graph of drillhole pXRF analyses for Si (left graph) and Al (right graph) over time (x axis), coloured by drillhole (red = CEH002, orange = CEH002, green =CEH003) and calibrations (blue) (calibrations using a Si blank standard).*

Readings are consistently 90 seconds comprising 30 seconds on each of Beams 1, 2 & 3. 61 readings are reported for QAQC purposes comprising a mixture of Calibration Checks (cal checks), Silica Blanks, and Standards (OREAS 2711A and OREAS 255B). Analysis of QAQC data indicates a drift of approximately 3% to 5% in readings for light elements including Si and Al over the period of analysis

of these three holes. Analytical data has not been corrected for this drift at this time, though the impact is not considered to be material to interpretations derived herein.

pXRF analysis does not give a reading for Na.

| Limit of Detection | Elements Analysed |
|---|---|
| <3,000 ppm | Mg |
| <400 ppm | Al, Si |
| <50 ppm | P, S |
| <25 ppm | K, Ca, Sc, Ti, V |
| <10 ppm | Cr, Te, La, Ce, Pr, Nd |
| <5 ppm | Mn, Fe, Co, Ni, Cu, Zn, As, Se, Rb, Sr, Y, Zr, Nb, Mo, Ag, Cd, In, Sn, Sb, Ba, W, Re, Au, Hg, Tl, Pb, Bi, Th, U |

*Table 5:* Elemental range and capabilities of the Vanta-M pXRF instrument.

Data is interpreted for lithochemistry and pathfinder chemistry purposes. To allow for broad filtering of data, readings are categorised as one of:

- L - lithological, being located to avoid intense alteration or mineralisation and primarily for a lithochemistry purpose.
- A - lithological, representing intense localised alteration, being partly for lithological and partly mineralogical purposes.
- T - target, being located to inspect chemistry of mineralogical, veining or intense fluid pathway features, being primarily for a pathfinder analysis purpose.

## 2.5. Magnetic Susceptibility

Magnetic susceptibility readings were collected on a half metre basis along each hole using a KT-10 instrument reading at $10^{-3}$ Kappa Units. A total of 2,588 readings were collected.

## 2.6. Structural Analysis

Drill hole survey control utilized Boart Longyear's TrueShot system, whilst core was orientated using their TruCore UPIX system.

Structure orientations were resolved utilizing CoreSolutions, a macro enabled Excel spreadsheet developed by CODES (University of Tasmania). Numbers of structural readings totalled: Veins = 451, 430 orientated, Planes = 818, 685 orientated, Folds = 52 and Faults = 203, 196 orientated. Structure data was compiled into faults, veins, folds and planar files (see appended files). Dip and dip direction structural notation convention is used.

Henty is a structurally controlled deposit. However, legacy drill hole structure data is scant and very poorly documented. Structure domains were simply defined as West of Henty Fault Zone (WHFZ) and East of Henty Fault (EHFZ). Ongoing evaluation has identified key structure orientations relative to currently defined domains herein. Future iterations of new structure data can be used to predict fault and vein distributions for both in-mine zones and exploration related geology.

Structure data was compiled into faults, veins, folds and planar files for CEH drill holes. Host Rock for each measurement was derived from DH_Geology tables. Initial potential structure domains were defined as HFZ_East and HFZ_West.

### 2.7. Rehabilitation

Two drill pads were constructed for (CEH001 & 002), and for CEH003. These pads are at the extreme northern end of the site and may be required for further geophysical assessment of the subject holes or for re-use drilling additional holes. Due to the highly variable terrain and the presence of protected vegetation species in the valley, it is also preferable to re-use sites as often as possible rather than opening new sites. For these reasons, the sites have been stabilised but not rehabilitated at this time.

To stabilise the sites, the collars have been capped, bark chips strewn across the site to reduce erosion, and the sumps left in place to act as settling ponds for run-off. At CEH002, the collar is stuck HWT casing. This hole intersected a low angle structural aquifer at around 15m depth and makes significant water unless restricted, so a steel cap has been welded on as the collar.

## 3. Results Achieved

The planned hole EDGI 1 was drilled as CEH001 (which failed at the Henty Fault) and CEH002. Drill sites for planned holes P2 & P5 were not cut because of difficulties establishing access. The pad for planned hole P4 was not cut because the hole was effectively negated by extending CEH002 to a greater than planned depth. The site for P3 was cut for CEH003 which was drilled to the south-west rather than east as planned. This redesigned hole sought to achieve the targets planned from site P2.

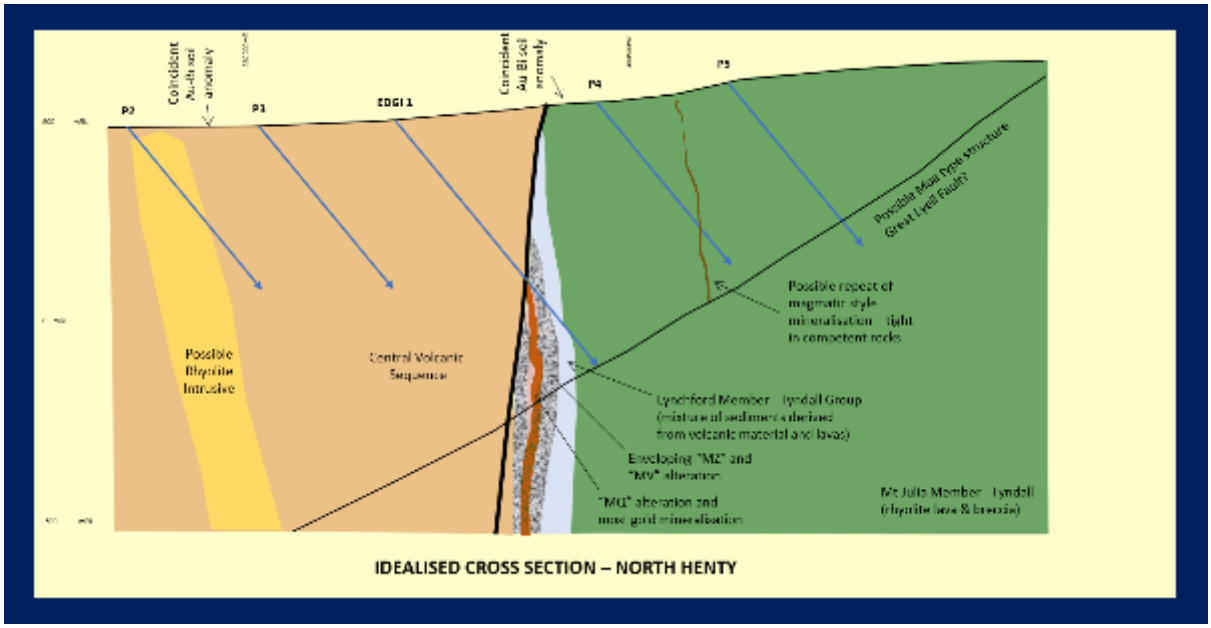


*Figure 5: Prognostic Section for EDGI Round 5 Grant application.*

## 3.1. Drilling

### 3.1.1. CEH001

CEH001 was designed as EDGI 1 (Figure 5) to drill the Henty Fault from west of the fault, test the typical position of Henty style mineralisation (within 50m east of the Henty Fault) and test for a potential low angled structure (analogous to the Moa Fault and possibly related to the Great Lyell Fault).

This hole failed when it intercepted the Henty Fault earlier than expected and struck a thick zone of gritty sand that could not be overcome. It was interpreted that the sand represented the intersection of two major faults (Henty and an unknown fault). The hole intercepted a sequence of moderate to strongly foliated dacitic volcanics and epiclastics interspersed with some potentially extrusive basalts and a number of intrusives amygdaloidal basalt dykes. The dacitic rocks are interpreted to be the Central Volcanic Complex (CVC) stratigraphy. Shallow east dipping to flat quartz-carbonate-chlorite veins with attendant selvedge chlorite-hematite-sericite alteration.

A foliated felsic volcanic at 101.5m contained several coarse red jasper-like grains on one band. It is interpreted that this may represent erosion of a distal exhalative source on this horizon and therefore a VMS style target.

*Figure 6: CEH001 at 79.8m showing peperitic textures in volcanic sandstone up-hole of a possible fold hinge.*

*Figure 7: CEH001 vein paragenesis examples showing left (@ 130m) Devonian buck quartz vein (up-hole) cuts quartz-carbonate-chlorite vein which overprints low core axis angle weakly banded silica-sericite vein with proximal pyrite selvedge which cross-cuts foliation; and right (@ 173.6m) foliation disrupting earlier carbonate-chlorite-pyrite-chalcopyrite vein.*

Basalt margins are often sharp and faulted, but locally feathered edged intrusive / peperite-like textures are apparent (Figure 12) indicating extrusion into an unconsolidated volcaniclastic sediment.

An extrusive lava was also observed, as well as potentially volcaniclastic basaltic facies. Banded bases and tops with more massive core to some intervals suggests high density mass flow emplacement is possible for some basalts, whilst other intervals are evenly fine grained and foliated/banded. Intervals of intercalated feldspathic dacite and basalt, representing interfingering volcaniclastic flows of different provenance. Leucoxene content/form is another discriminator, being common and flattened on foliation in the volcaniclastics, and more broadly disseminated and less deformed form in interpreted coherent basalts.

Major fold closures are evident from foliation and extensive quartz veining at 113-114m & 126-129m. The broad interval of these examples is likely representative of a significant anticlinal closure. Up and down hole are repeats of (sulphidic and base metal anomalous) ashy sericitic units stratigraphically overlain by pervasive silica-albite alteration zones with opposing facings. Parasitic Z-style folding downhole hole at 223.7m (Figure 8) provides support suggesting a west vergence to an anticline.

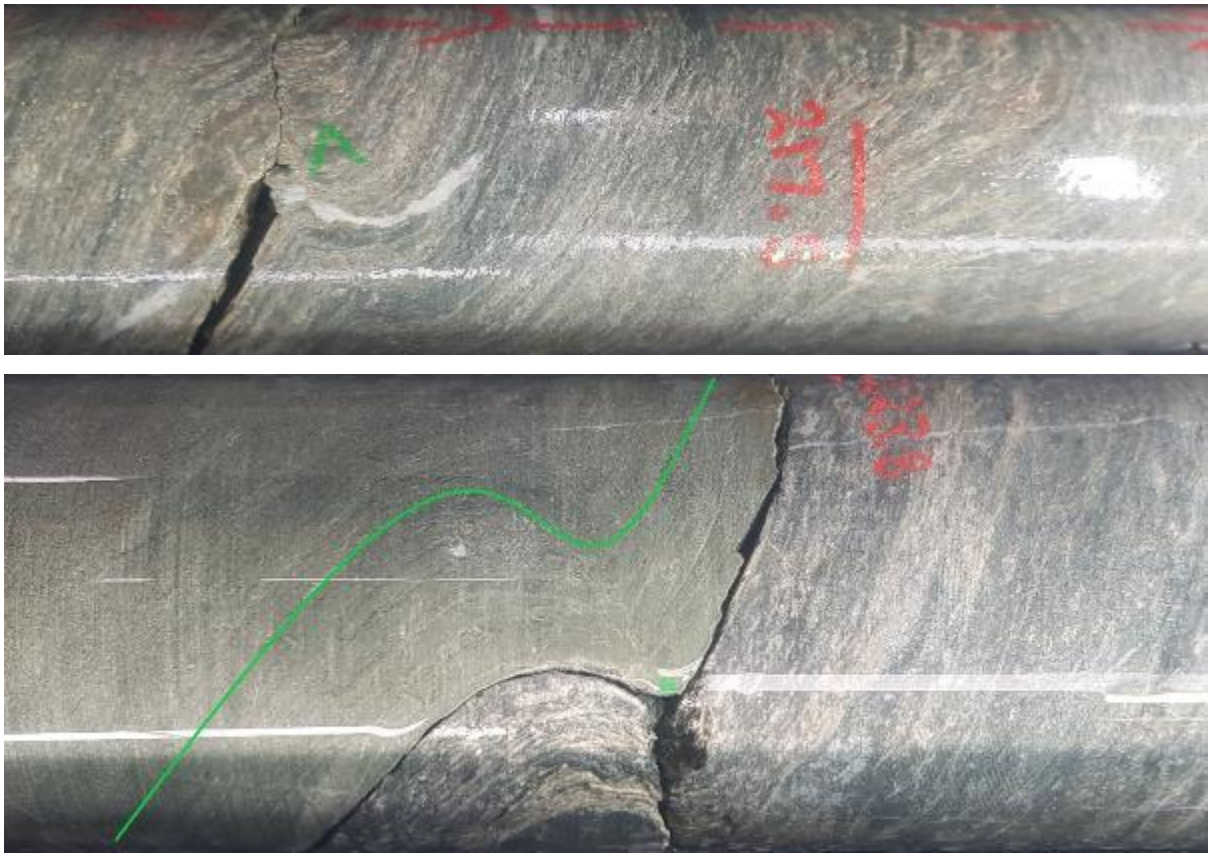

*Figure 8: CEH001 at 217.44m (top) and at 223.77m (bottom, plunging -10° towards 212°TN) showing Z-style parasitic folds with vergence to an anticline up-hole. The fold plunge likely reflects Henty Fault related/proximal folding, as compared to the more regional Devonian 150° fold hinge plunge / strike trend. The carbonate vein show (top) is emplaced pre-folding, foliation and sericite development.*

### 3.1.2. CEH002

The second attempt to complete proposed hole EDGI 1 was drilled from the same location as CEH001 with an azimuth approximately 15 degrees north of that hole to avoid the structural complications it intercepted. CEH002 successfully penetrated the Henty Fault Zone and was continued to a total depth of 735m to investigate features of interest identified along the way. These features were principally zones of intense sericite alteration, proto-shear development and a zone of prospective Lower Tyndall rocks identified towards the end of the hole.

On the western side of the Henty Fault (to 240.5m), CEH002 intersected the same sequence of basaltic and foliated dacitic rocks of the CVC package as CEH001 and commentary is generally the same as for that sequence. Basalts in CEH002 are variably altered with the strongest altered basalts typically bleached in appearance, variably sericitic and often containing fine sulphide veinlets. One 15cm example of the bleached appearing end member basalt intrudes MJM rhyolite east of the HFZ at 391.75m, indicating that similar basalt alteration processes were active on both sides of the HFZ. This observation potentially dates many of the basalts on the west as Late Cambrian – Early Ordovician at the earliest. These basalts could correlate to post extrusive facies of CVC Spillway Basalt Breccia or possibly to the Tyndall Group Upper Howards Basalt Breccia. Intrusive basalt contacts are commonly faulted with slickensides and ramps indicating two fault movements in some cases.

An alteration feature of special note occurs at 104.5m where the basal contact of an amygdaloidal basalt is relatively more foliated and sericitic with stretched amygdales. The more altered area lacks leucoxene, which is abundant in less foliated basalt up-hole, indicating fluids associated with sericite alteration are involved in moving titanium.

East of the Henty fault (from 276m), the hole intersected a rhyolitic conglomerate and volcaniclastic sandstone sequence to 335m. This sequence is only weakly polymict and dominantly comprised of quartz phyric rhyolite, indicating it may be a Mount Julia Member correlative rather than the Zig Zag Hill Member. This observation is inconsistent with stratigraphy in an equivalent position in holes further south.

*Figure 9: Photo of CEH002 at 532.1m showing cream to grey laminar banded, medium grained crystal rich volcaniclastic sandstone, coarsening downhole and with potential relict truncated crossbedding indicating up-hole facing.*

The hole intersected primarily quartz phyric rhyolitic volcanic from 335m to 597.5m (Figure 9) with minor intervals of epiclastic and altered basalt. A coherent interval of intense sericite alteration was identified between 414.3m to 474m, possibly representing a hydrothermal fluid pathway. The rhyolite has traditionally been considered to be Mount Julia Member, however, may represent Suite 2 Porphyry that is found south of the mine. The rhyolite primarily appears intrusive but this nature is

unclear. Folded carbonate veins between 433 to 459m depth indicate the stratigraphy was subject to hydrothermal alteration pre-Tabberabberan Period.

At 460.8 to 460m, CEH002 intersects a silica-fluorite-pyrite veined interval of fault breccia. The fluorite post-dates the breccia and cuts silica-sericite altered clasts but is also locally enclosed by strong sericite foliation indicating two sericite events.

From 597.5m to 605.4m the hole intersected amygdaloidal basalt encompassing a major brittle fault and associated intense carbonate veining near its downhole contact. Fine grained andesitic epiclastics continue to 618.05m depth.

*Figure 10: CEH002 at 352m showing coarse grained quartz-feldspar phyric massive coherent rhyolite lava.*

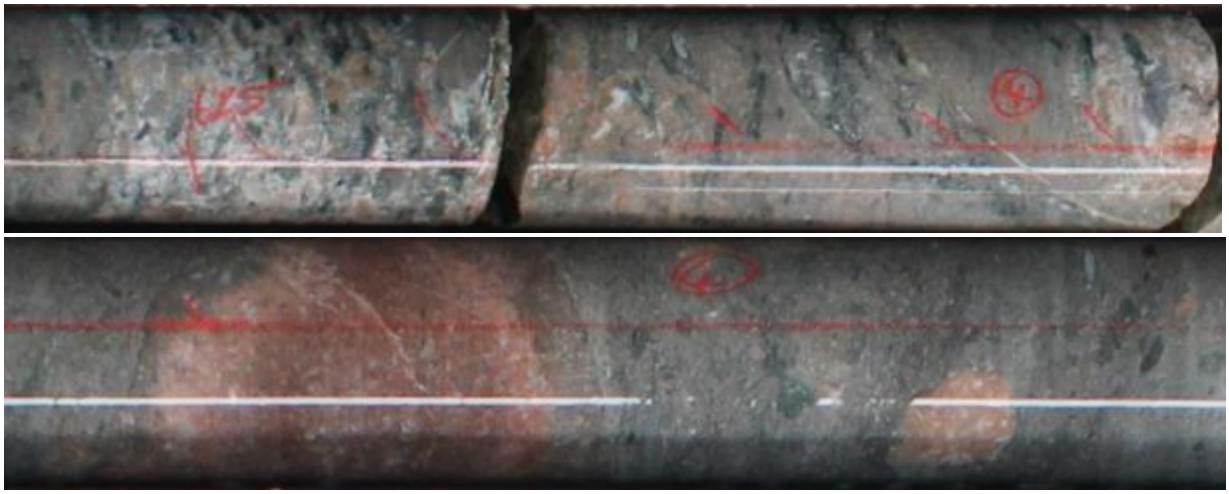

*Figure 11: CEH002 at 625.1m (top) and 630.2m (bottom) showing polymict lithic volcaniclastic interpreted as a correlative of the Lower Tyndall Lynchford Tuff.*

From 618.05m to 634.5m the hole intersected a polymict lapilli lithic andesitic volcanic breccia that compositionally strongly resembles a correlative of the Lower Tyndall Lynchford Tuff with common chloritic fiamme textures (Figure 11). The unit contains common scattered albite silica altered quartz and quartz-feldspar-phyric rounded rhyolite clasts ranging up to large lapilli size (~10cm max) and rare grey silica and chert accidental lithic clasts. This intersection is critical for the hole as it relates the stratigraphy back to the known Henty Mine stratigraphy. Specifically, mineralisation in the Darwin Lodes is found slightly downhole (usually <50m west) of the Lynchford Tuff.

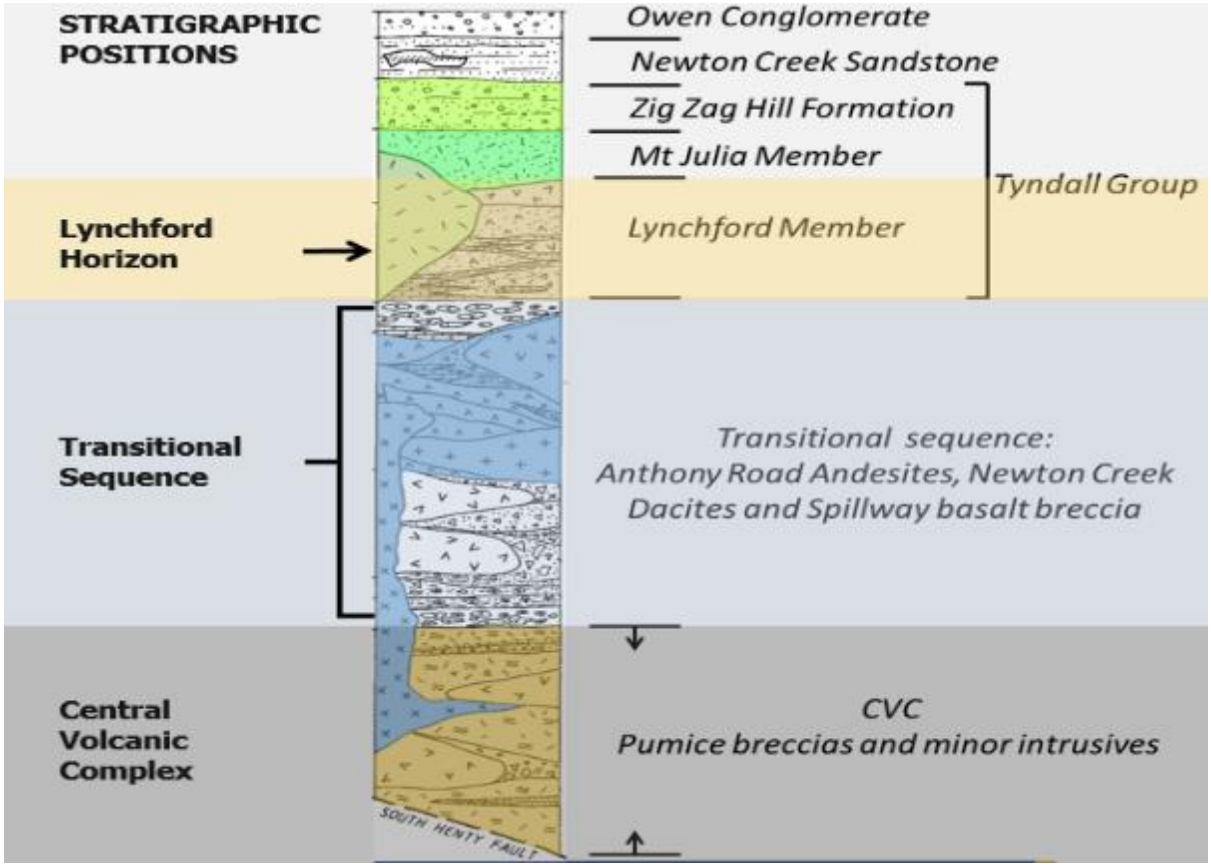


*Figure 12: Interpreted Mount Read Volcanics Stratigraphy*

Beyond the interpreted Lynchford Tuff, the hole intersects more quartz-phyric rhyolite with several intense coherent alteration zones interpreted as ABSI (albite-silica) and sericite alteration. The contact between Lynchford Tuff and rhyolite is occupied by a quartz-chlorite vein so the nature of the contact cannot be discerned.

Moderate to strong foliation west of the Henty Fault and in sericitic altered areas of quartz-phyric volcanics east of the Henty Fault are common.

Veining is generally flat to shallow east dipping.

### 3.1.3. CEH003

CEH003 was drilled to the south-west to intersect the targets in the western footwall of the Henty Fault planned from site P2. These targets included an interpreted north-west oriented structure coincident with multi-element soil anomalism including Au, Ag, Bi and Sb. A coincident significant potential structure wrapping into the west side of the Henty Fault was also interpreted from Lidar data. It was also conjectured that an intrusive rhyolite body interpreted to cross and terminate the northern end of the Henty mineralisation may be present in this area.

The hole intersected a series of intercalated dacitic volcanics, volcaniclastics and epiclastics and intruded basalt dykes.

### 3.1.4. Fluid Pathways

Two significant fluid pathways are identified in CEH002. These are from 414.3m to 474m and from 635m to 647.6m downhole. Both zones are located within competent quartz-phyric rhyolite and are

represented by intense sericite-silica±carbonate alteration (mica probably muscovite) and associated with increased peripheral hydrothermal carbonate veining.

There is no clear fluid pathway in close proximity to the eastern side of the Henty Fault where Henty style mineralisation is generally identified. No significant fluid pathways were identified in CEH001 or CEH003.

### 3.1.5. Major Structural Features

The Henty Fault (247m depth) was the only significant structure intercepted in CEH001. The hole terminated in sandy material at 255.1m. No significant structures were intersected in CEH003.

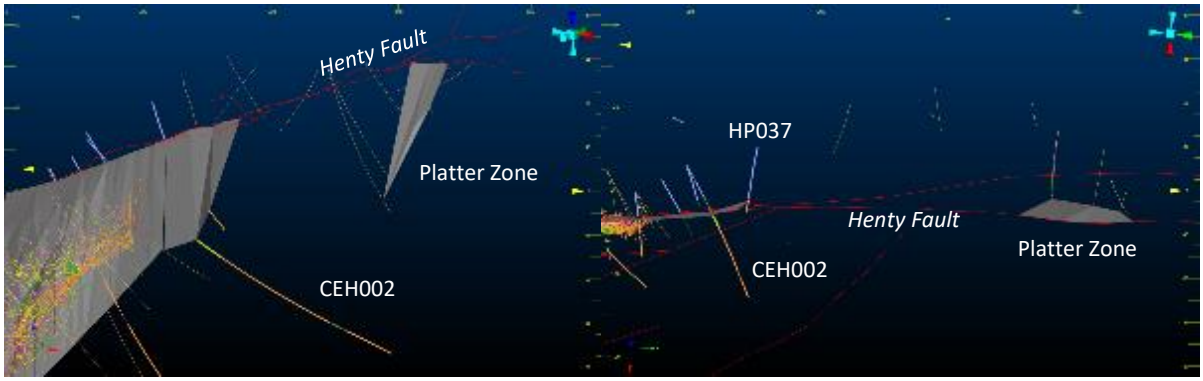


*Figure 13: NNW (335°) facing oblique view of wireframe of the Henty Fault Zone (left) and plan view of Henty Fault Zone (right) including lateral extension at the Platter Zone, demonstrating NW oriented flexure in HFZ identified by EDGI drilling.*

Major structures intersected in CEH002 include:

- 11.1-11.5m; probable low angle fault, interpreted to be a shallow high flow structural aquifer.
- 143.2-143.4m; small fault that juxtaposes similar lithologies but presenting different structural domains. Contains a 5cm indurated cataclastic fault and 15cm of chevron folded epiclastic material bound by shearing.
- 241.9-275.2 (33.3m); Henty Fault comprising abundant intervals of up to 0.5m of cataclastic pug filled brittle faulting, brittle and ductile shearing, indurated healed older faulting zones, and open to tight and chaotic folding. Locally overprinted by late fuchsite alteration.
- 275.2-314.3m (39.1m); zone of high structural deformation attendant to the Henty Fault comprising consistent high density of strongly broken rock, fine to moderate late puggy brittle movement zones, older indurated healed faults, and common proto-shear development with domained mineral separation based on structural competence.
- 602-604.5m; Recent puggy fault within basalt intrusive, possibly reactivation along an earlier plane of weakness utilised by the basalt.

The intersection of CEH002 with the Henty Fault was slightly earlier in the hole than anticipated from straight projection north of the fault from other drilling. The next hole to the north in which the fault is intercepted is HP037. The location of the intercept in that hole relative to CEH002 indicates that the fault has taken a significant north-west oriented deviation between these two holes (Figure 13). It is likely this deviation is associated with the extreme degree of attendant faulting intersected in CEH001 & 002. The Henty Faults have been mapped as separating further north of this location. Drilling intercepts of the eastern Henty Fault further north at the Platter Zone demonstrate that the Henty Fault has resumed its prominence on the eastern fault line. These results indicate the Henty

Fault is more complex in the area north of CEH002 than is currently recognised. Further mapping is required to elucidate this point.

## 3.2. Geochemistry

Conventional and pXRF geochemistry results from CEH001, 002 & 003 were assessed for lithochemistry and pathfinder element purposes. All geochemical data (ICPMS & pXRF) presented in this report can be interpreted referring to Table 6 as key for attributions.

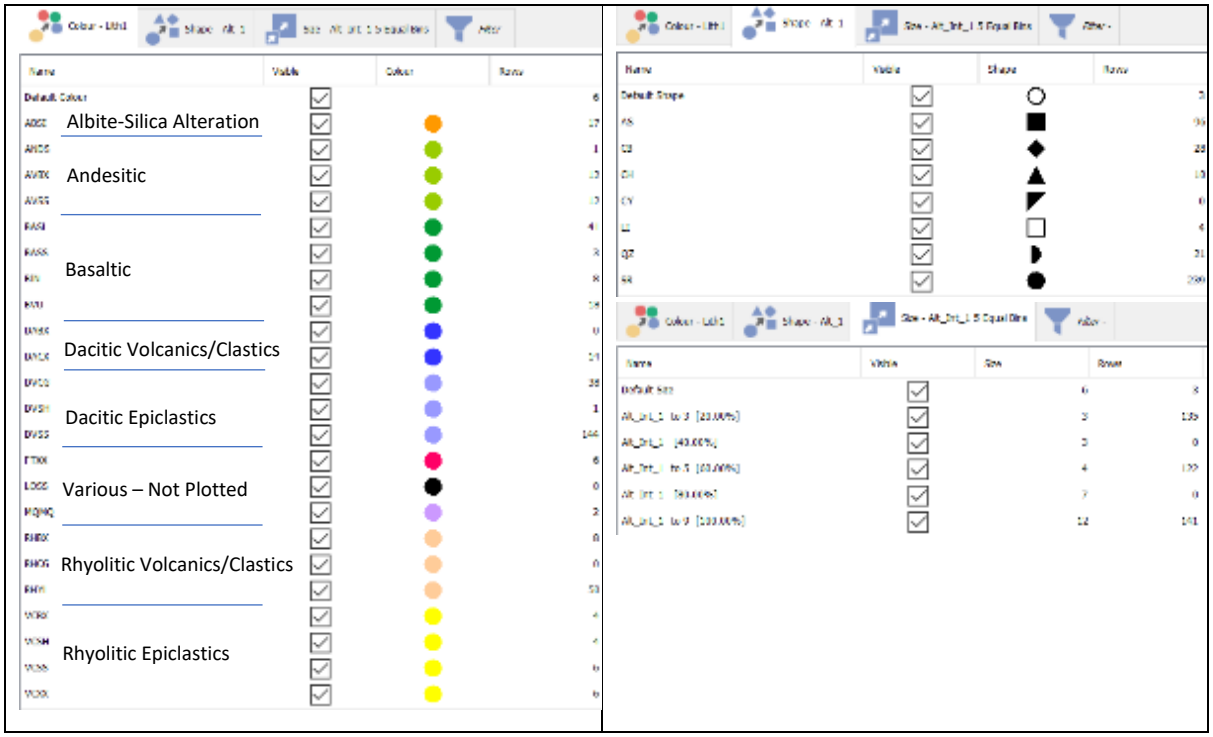


*Table 6: Legend for all geochemical data presented in this report.*

All pXRF geochemistry readings are point analyses, taken with an 8mm scanning window onto round core. A selection of samples analysed as 'target' samples, being targets of interest and not taken for lithochemical purposes, have been excluded from the lithochemical analysis herein.

### 3.2.1. Lithochemistry

In Figure 14, an interval in hole CEH003 is used to demonstrate a direct comparison between ICPMS and pXRF data for select elements used in lithochemistry analysis. Although the reported elemental abundances differ for each element between the two data sets, the relative abundance is generally consistent. The amplitude of changes in elemental abundance are broadly consistent between the two data sets except for Fe & Ti, however this discrepancy has not been material to the lithochemical

interpretation. Rock discrimination using Ti, Zr, Nb & Y has generated similar results in both data sets

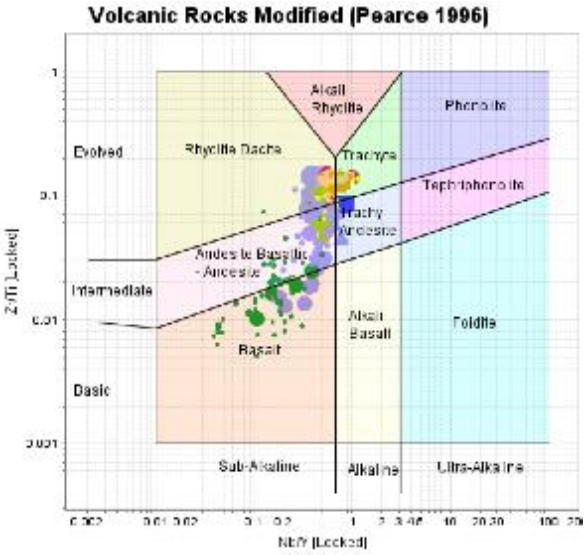


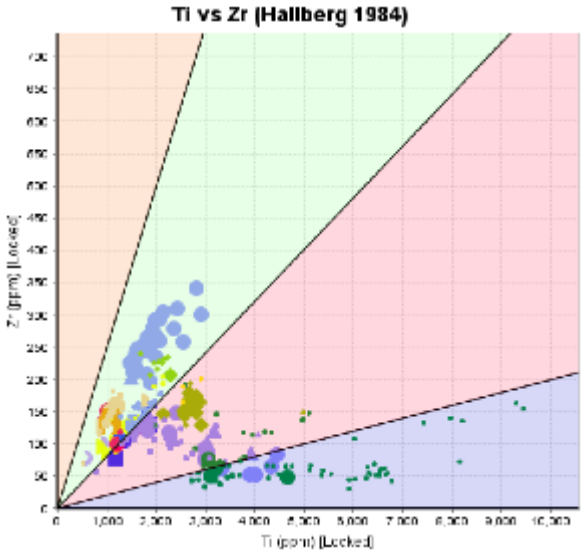


(

Figure 15, Figure 16, Figure 17).

The noisier response in pXRF data is due to the point sample nature of the readings. Some readings return below detection results for Nb and can't be used for Ti-Zr-Y-Nb rock discrimination (Figure 18). Assessing Ti, Zr, Nb & Y data, the rocks analysed in this study present as dacite, andesite and basalt. The rocks that petrogenetically appear to be rhyolitic facies present on discrimination diagrams as trachyte due to the ratio of Nb/Y present, however there are no obvious trachytic rocks identified.

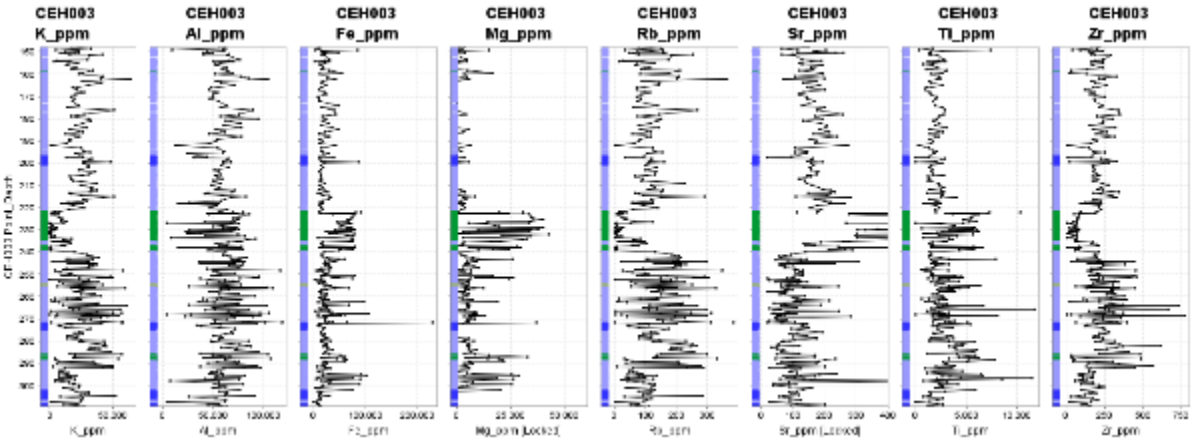

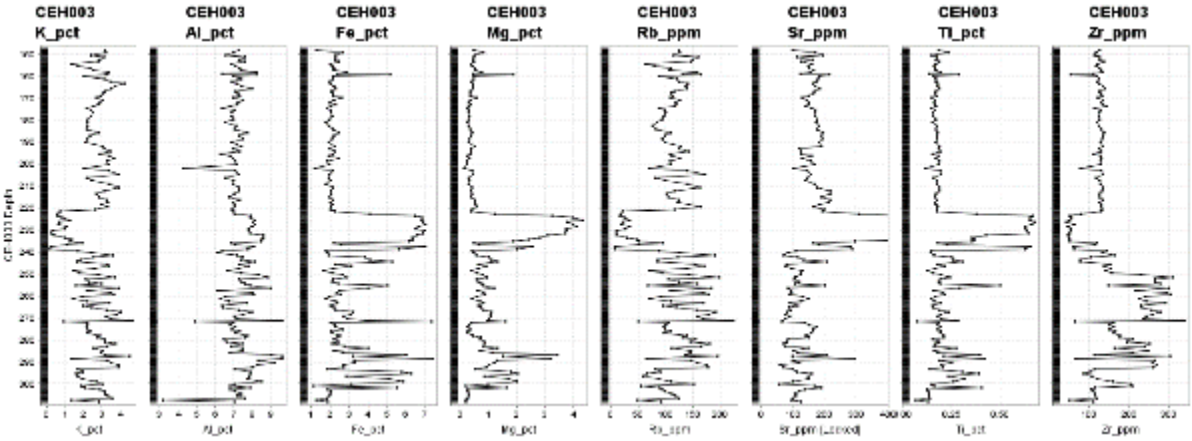


*Figure 14: Comparison of select downhole chemistry for hole CEH003 contrasting results from pXRF (top row) and ICPMS (bottom row).*

Assessment of samples from core logged as dacitic affinity identifies that a majority of the population plots as dacite, possibly trending towards andesitic composition, particularly in the volcanics. A smaller population of dacitic rocks plots as basalt and is likely mis-logged. The samples this second population represents are found proximal to basalt on the western side of the Henty Fault. A third dacitic population on the Ti-Zr plot in Figure 15 shows a population which appears to be transitional from basaltic to dacitic. There is no clear spatial correlation with this last population.

Assessment of samples from core logged as andesitic affinity indicates they dominantly plot as andesitic, though there is a small population that plots as dacitic. All of the andesite population that plots as dacitic is located within the andesite interval between 606m to 634m in CEH002.

Assessment of samples from core logged as rhyolitic affinity indicates some variance between ICPMS and pXRF data sets. Results of ICPMS data provide a tight population cluster within the dacitic field, while results from the pXRF data (significant larger population) plot predominantly within the dacitic field but also transgressing (evolving) to the andesite field in Ti-Zr plots (Figure 15). There are also a small number of outlier pXRF reading results in the rhyolitic and basaltic fields. These latter results are likely inaccurate due to low element input values. Assessing the data in Zr/Ti against Nb/Y plots, the ICPMS data indicate a trend towards trachytic composition (Figure 15) which is not strongly reflected in the pXRF data (Figure 17). Rhyolitic epiclastics are not represented in ICPMS data. In pXRF data, this group presents as a dominantly dacitic composition (Figure 15).

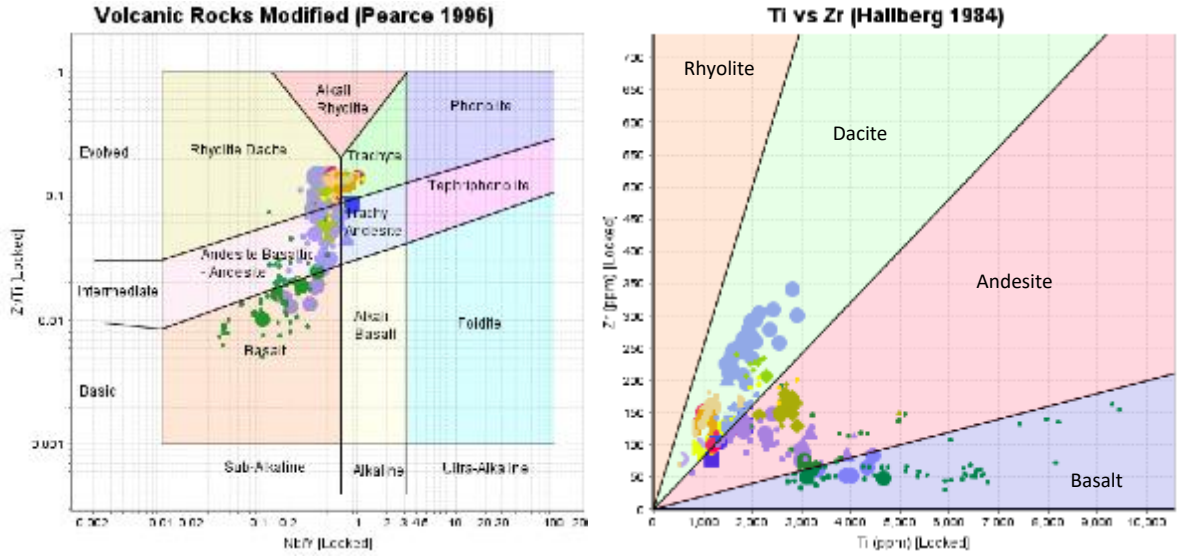


*Figure 15: Rock classifications of ICPMS data for drillholes CEH001, CEH002 & CEH003.*

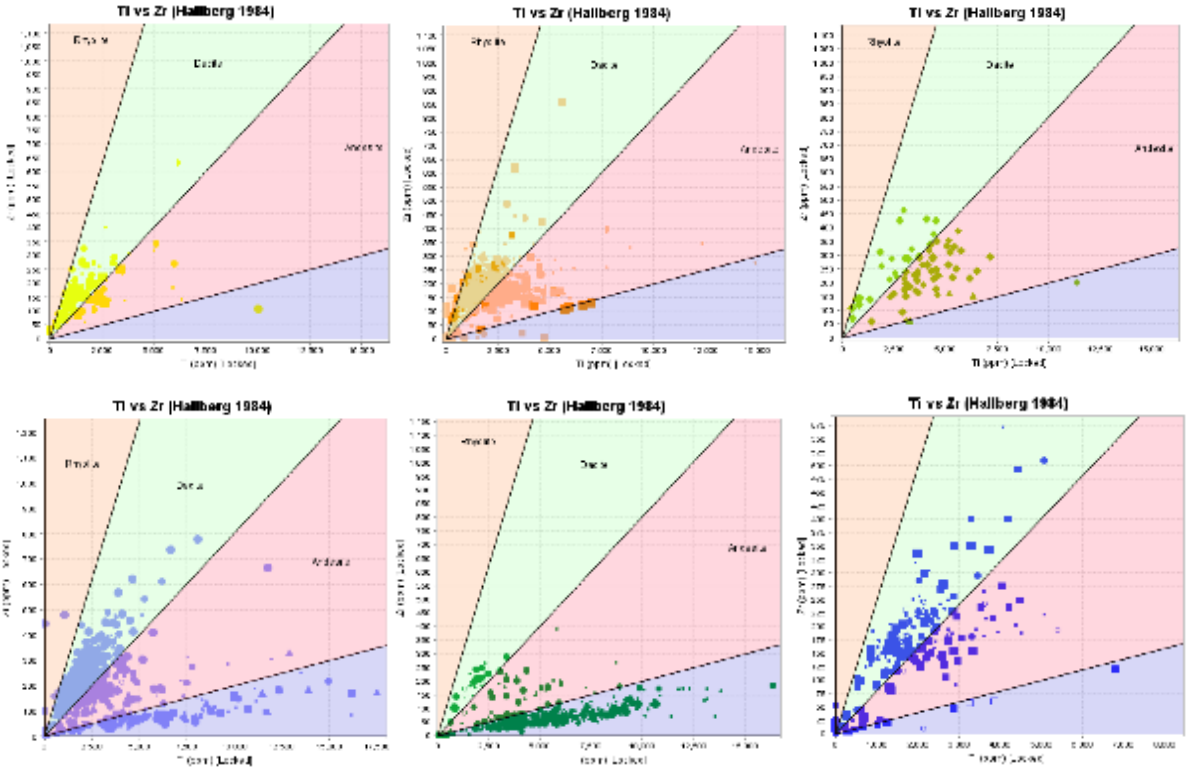


*Figure 16: Ti-Zr diagrams (using Hallberg 1984 format) for pXRF data sequentially presenting core logged as Volcanic epiclastic & breccia, Rhyolitic, Andesitic, Dacitic crystalline tuff & breccia, Dacitic epiclastic, Basaltic.*

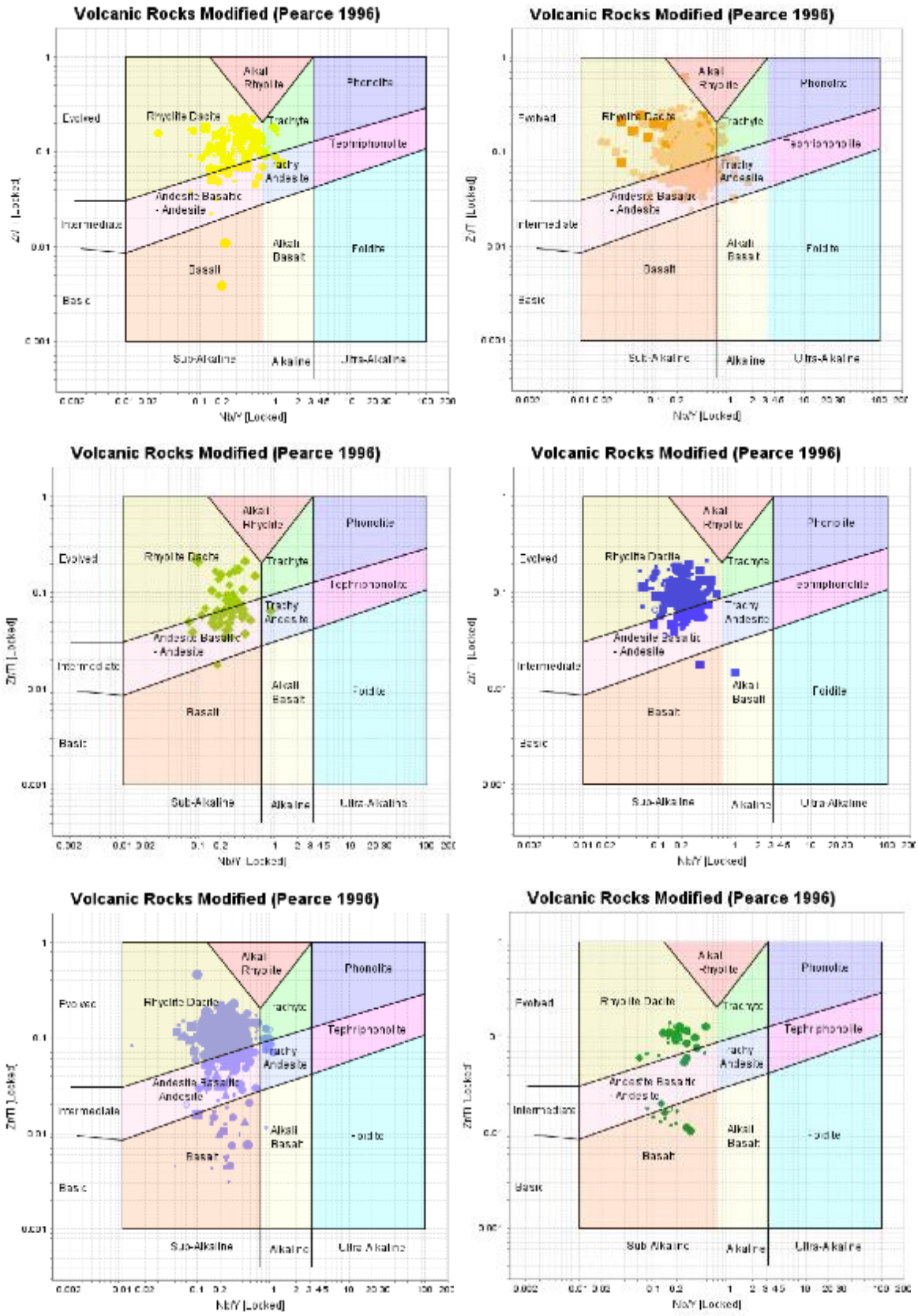


*Figure 17: Volcanic rock classifications (using a modified Pearce 1996 format) for pXRF data sequentially presenting core logged as Volcanic epiclastic & breccia, Rhyolitic, Andesitic, Dacitic crystalline tuff & breccia, Dacitic epiclastic, Basaltic.*

Assessment of samples from core logged as basaltic affinity indicates the majority of basalt samples are of basaltic affinity with a range of immobile element values all with a high correlation in their ratio of Ti/Zr abundance. There is a secondary basalt population plotting with andesitic to dacitic composition which are likely to be mis-logged core. Although most of the basaltic units intercepted display hypogene characteristics, some may be of epigenetic character and a source of the occasional basaltic content in the epiclastics. Petrology is required to further elucidate this supposition and properly characterise the CVC units.

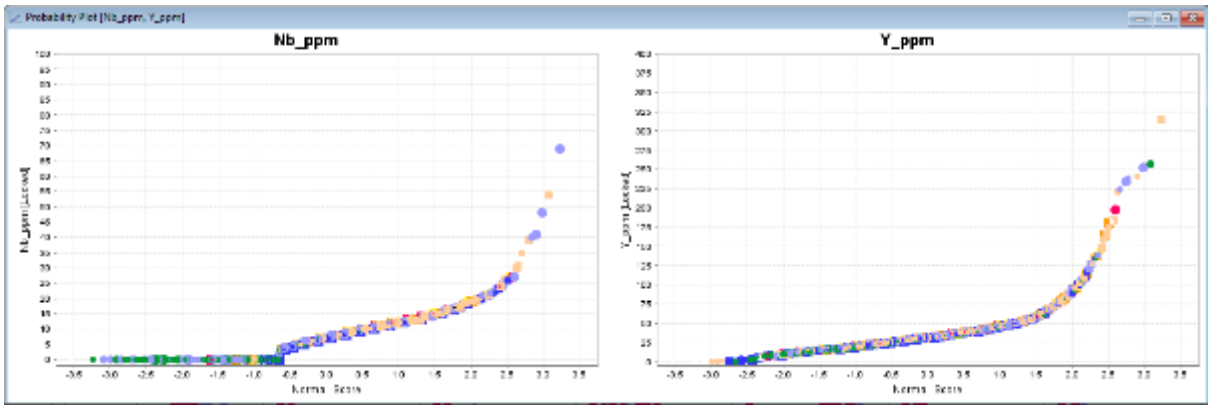


*Figure 18: Probability plots for Nb & Y data*

We conclude that although there are some subtle differences between elemental ratios of Ti/Zr & Nb/Y in the core studied here, there is no clear way to discriminate lithologies other than basalt, and therefore no clear way to discriminate CVC from Lower Tyndall stratigraphy using just these vectors.

No conclusion is drawn here for observation that petrogenetically rhyolitic rocks are plotting as dacitic composition. This matter will be addressed in further studies. Assessment of alumina saturation for the samples (using ICPMS data) (Figure 13) demonstrates that basaltic, andesitic and dacitic volcanics are metaluminous. Rhyolite and some dacitic samples show a peraluminous nature, indicating fractionation of the volcanics over time. The more peraluminous samples are calc-alkaline in nature, tend more towards muscovite alteration.

#### 3.2.1.1. Lithochemical Discrimination

A range of other techniques were tested with the EDGI dataset to discriminate lithologies and stratigraphy. The dataset contains Tyndall and CVC stratigraphies, late intrusive dykes, and younger mafic intrusives. Effectiveness of this particular dataset to test stratigraphic discrimination is limited however as the Lower Tyndall in these drillholes does not contain dacite, and there is no rhyolitic facies observed in the area in the CVC. Therefore, no direct comparison can be drawn within this dataset between the two different stratigraphies.

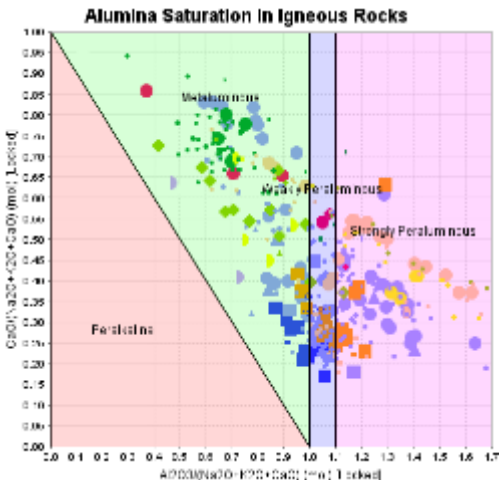


*Figure 19: Alumina saturation diagram showing all holes using ICPMS data.*

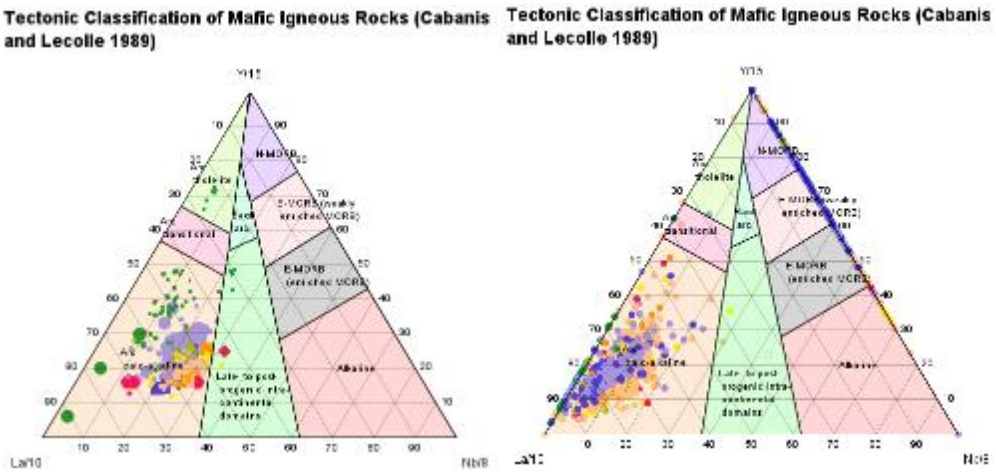


*Figure 20: Tectonic classification of EDGI data sets demonstrates most of the core analysed is Arc calc-alkaline, though some basalt samples present as tholeiitic. ICPMS date on left, pXRF on right.*

The lithologic discrimination diagrams which delivered successful results are:

- The Pearce (1996) diagram utilised in Figure 15 & Figure 17 is a modified version of a log Nb/Y Vs log Ti/Zr diagram used as an immobile element proxy for the TAS diagram for discriminating volcanic rocks for massive sulphide exploration.
- Hallberg (1984) plots use the ratio of immobile elements Ti & Zr to classify volcanic rocks primarily in deeply weathered terrain. The technique is a useful tool in altered and unweathered terrains as well.
- Cabanis & Lecolle (1989) use La, Y & Nb to discriminate the tectonic setting of volcanic series and identify crustal mixing and / or contamination.
- The Jensen Cation Plot is a classification system for subalkaline volcanics using proportions of cation abundance including Ti, Fe, Mg & Al (Rollinson 1993). The method is particularly useful for komatiites, however it is a useful discriminator for calc-alkaline to tholeiitic series as well.
- The Hastie et al (2007) diagram for classifying altered volcanic island arc rocks. Th and Co are used as proxies for K2O and SiO2 respectively, with Th content being used to sub-divide rocks into volcanic series (tholeiitic, calc-alkaline, High-K calc-alkaline and shoshonitic). Gradual removal of Co from the melt during crystallisation of subvolcanic island arc rocks reflects fractionation from basalt to rhyolite, as shown in the field boundaries for different rock types along the x-axes.

Plots such as the Tectonic Classification of Igneous Rocks (Cabanis & Lecolle 1989) (Figure 20) demonstrate that the majority of the rocks present in this core are calc-alkaline Arc derived rocks. The difference in sensitivity between ICPMS analyses and point sample pXRF readings is clearly shown between the two diagrams in the figure, indicating XRF data is not as reliable for using this discriminator as ICPMS data. Both diagrams however show a gradual evolution towards a Late to post-orogenic intra-plate classification as the volcanics evolve towards rhyolitic composition. A small sub-population of basalt samples plot as tholeiitic in composition. The Tectonic Classification diagram provides a very similar result as using a Hf-Rb-Ta diagram for discriminating granites. It is possible the diagrams may be used interchangeably where alteration has impacted the input elements.

The Jensen Cation plots in Figure 21 provide the best sensitivity for discriminating relatively unaltered lithologies of any of the trialled discrimination diagrams. Using ICPMS data, the rocks plot primarily as calc-alkaline volcanics with a small population of high Mg tholeiitic basalt and other tholeiitic species.

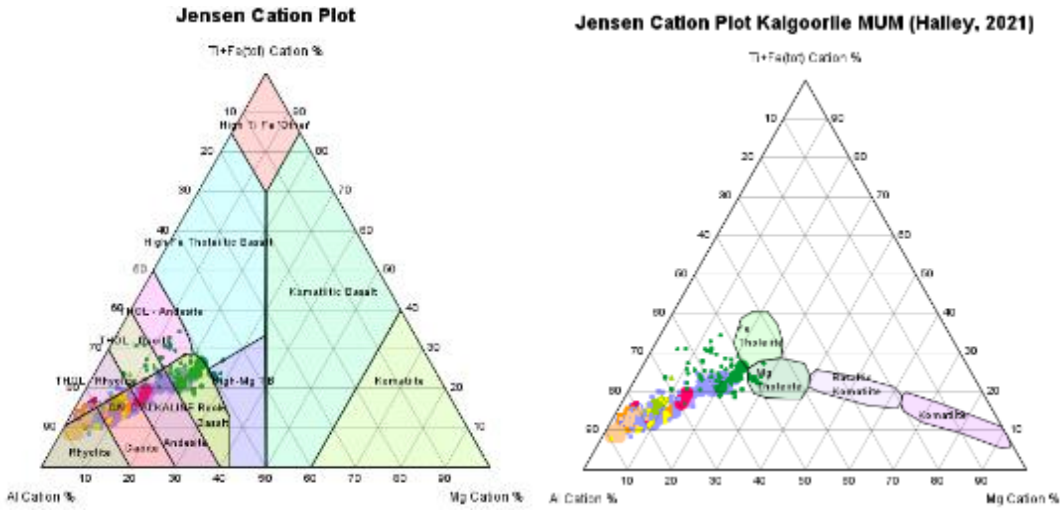


*Figure 21: Jensen Cation Plots for discriminating lithologies. ICPMS data only.*

The high Mg tholeiitic basalts represent the Late magnetic basalt on the eastern side of the Henty Fault in CEH002, and a correlatable high Mg, Ni, Co, Fe, Sc, Sr, Cu basalt in CEH002 & 003. The same basalt plots as firmly calc-alkaline affinity on a Th-Co discrimination plot (Figure 22), as all of the Late to post-orogenic intra-continental and tholeiitic basalt sampled on the Tectonic Classification diagram (Figure 20), and as the high Ti samples on a Hallberg Ti-Zr diagram (Figure 15). It is concluded this basalt is late in the paragenesis and could be used for zircon dating to bracket the upper limit of mineralisation as it is not altered by mineralising fluids.

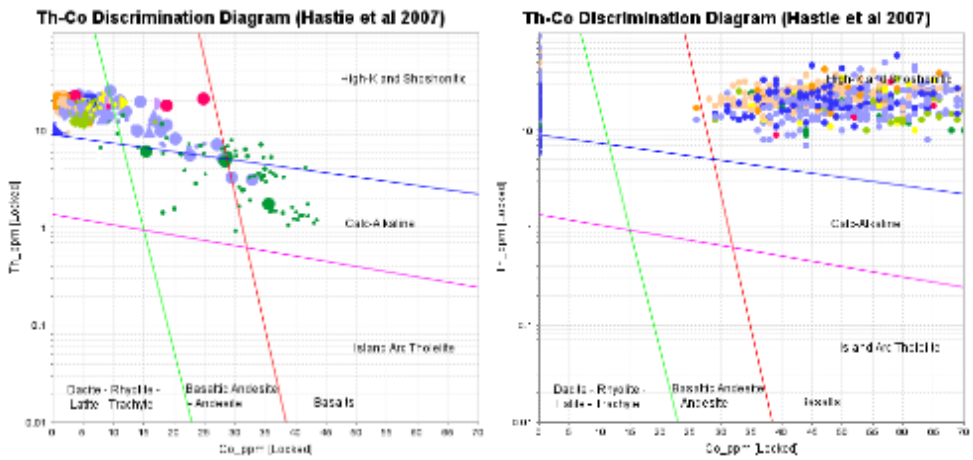


*Figure 22: Th-Co Discrimination Diagram for classifying altered volcanic arc rocks. ICPMS on left, pXRF on right.*

The Jensen Cation plot discriminates rhyolite from dacite based on the relative abundance of Al. The samples plotting as rhyolite on the Jensen diagram include those rocks logged as quartz-phyric rhyolite, and a proportion of the rocks logged as dacite from the CVC stratigraphy. The rocks logged as andesite plot within the dacite field in this diagram and in the Hallberg Ti-Zr diagram (Figure 15). When using pXRF data on this plot, the spread of the data is much greater and extends broadly across

the calc-alkaline and tholeiitic fields as the instrument does not have sufficient sensitivity to generate useful data for this discriminator.

The Th-Co discrimination diagram of Hastie *et al* 2007 (Figure 22) provides a further refinement on the Jensen plots of Figure 21, identifying that the Lower Tyndall and CVC volcanics tend towards High-K to Shoshonitic composition. The basalts plotting in the calc-alkaline field are primarily the High-Mg basalts identified in the Jensen plots (Figure 21). The right-hand image in Figure 22 is the same plot using pXRF data which demonstrates that the pXRF instrument does not have sufficient sensitivity to utilise on these plots and provides misleading results.

Porphyry prospectivity plots (Figure 23) demonstrate that the volcanics are not prospective for porphyry style mineralisation. The High-Mg basalt has higher V/Sc and Sr/Y ratios than the other rocks and plots higher in these diagrams but is still not prospective. Rocks logged as andesitic demonstrate a substantially lower V/Sc ratio, indicating they may be unrelated to The Tyndall Group rocks. The Tyndall Group rocks demonstrate increasing magnetite fractionation as volcanics evolve towards more dacitic and rhyolitic compositions.

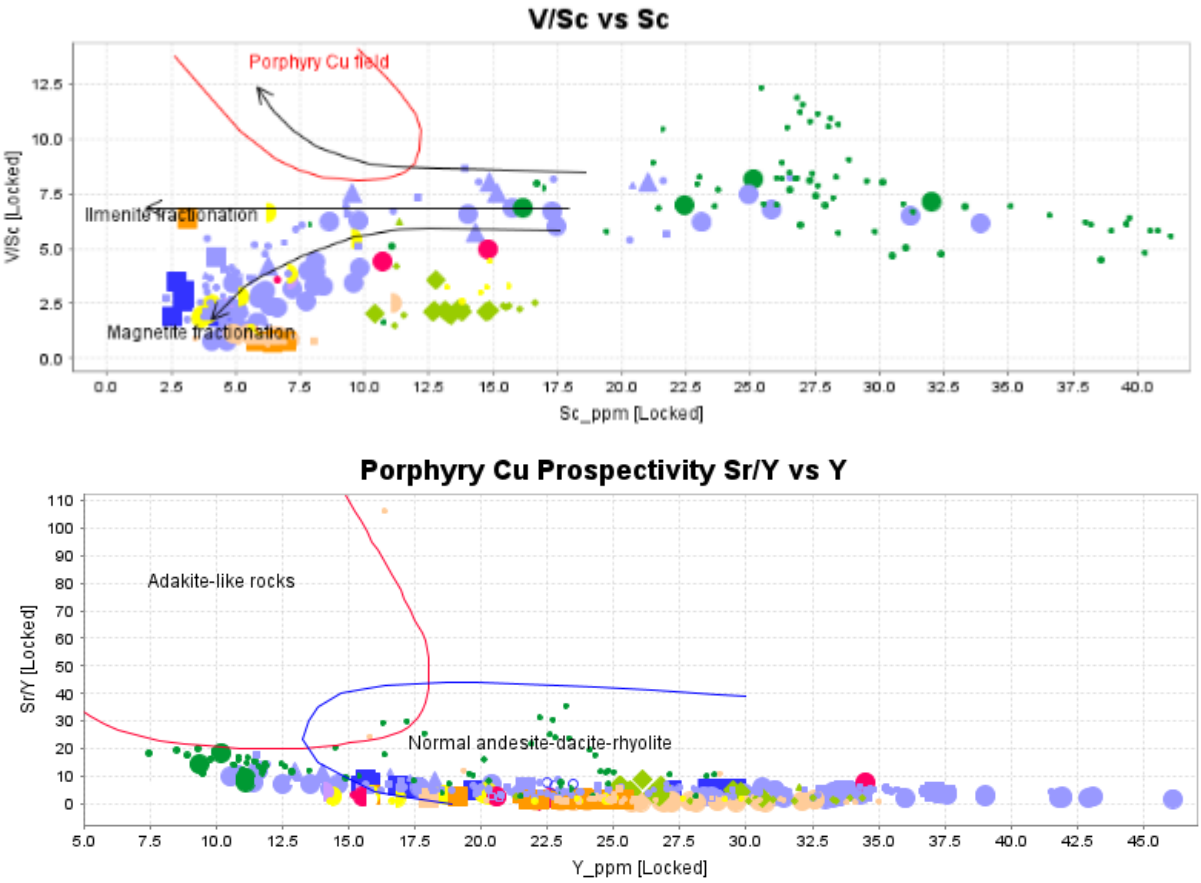


*Figure 23: Porphyry prospectivity plots for Henty volcanics*

By analysing the geochemical data with a series of lithological discrimination diagrams, it is found the volcanics and basalts of the CVC and Lower Tyndall are High K to shoshonitic calc-alkaline volcanics demonstrating a continuous broad evolution from basaltic through andesitic and dacitic to rhyolitic compositions. There is a Late High-Mg tholeiitic basalt identified in holes CEH002 & 003. Andesite

identified in CEH002 may also be later than the surrounding volcanics. The Henty volcanics (both Lower Tyndall and CVC) are not prospective for porphyry style mineralisation.

#### 3.2.1.2. Intra-Lithology Discrimination

Assessment of small variations in elemental composition in relatively homogenous lithologies can provide moderate confidence discrimination of individual units within lithologies, giving insight to volcanic evolution and stratigraphic facing.

Downhole plots of elemental abundance (pXRF data) in CEH002 (Figure 24) demonstrate gross changes in lithology as well as giving indication of magmatic evolution within the rhyolitic lithology. Several elements (especially Ca, Si, K, Rb, Sr) clearly discriminate rhyolitic facies from dacitic facies, indicating that core intersected in the Henty Fault Wedge between the two Henty Faults (red samples) has been mis-logged as dacite (CVC) when it is of rhyolitic composition (Lower Tyndall Group). But trends in the gross abundance of some elements (increasing Si, Al, K & decreasing Sr, Ca, Ti) show increasing fractionation of the rhyolitic facies up-hole, likely representing apparent younging to the west (or obliquely up). Other elements including Zr, Nb & Y do not appear to change elemental abundance over the intersection.

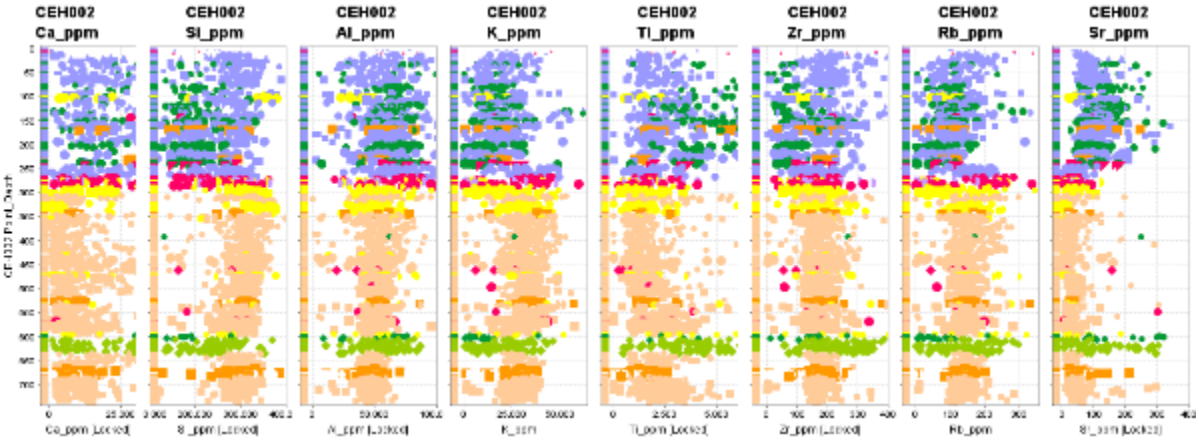


*Figure 24: CEH002 downhole plots of key elements demonstrating evolution of rhyolitic facies towards the west (inclined hole drilled west to east). Downhole plots have been restricted to around the 80th percentile of data to highlight trends in mean distribution.*

Further assessment of geochemical data for CEH002 using univariate wave tessellation analysis shows that small changes in elemental abundance can be used for discriminating inter and intra-lithological variation. In Figure 25, Fe, Sr & Ti clearly highlight the stratigraphic boundary between CVC and Lower Tyndall (dacite Vs rhyolite) at 249m depth and highlight mafic facies around 600m depth. The contacts are consistently defined across multiple elements. The distribution of K, Si and Al highlight the change from Zig Zag Hill rhyolitic epiclastics to quartz-phyric rhyolite (potentially of the Mt Julia Rhyolite member).

All elements presented in Figure 25 show that the rhyolite below 625m depth is of slightly different composition to the rhyolite above 600m depth. This observation is critical as these two rhyolites are separated by a major fault, a Late High-Mg basalt, and an intersection of (logged) andesitic material and interpreted Lynchford Tuff. It is inferred that there is significant juxtaposition of rhyolites of differing fractionation states on either side of this non-rhyolitic intersection.

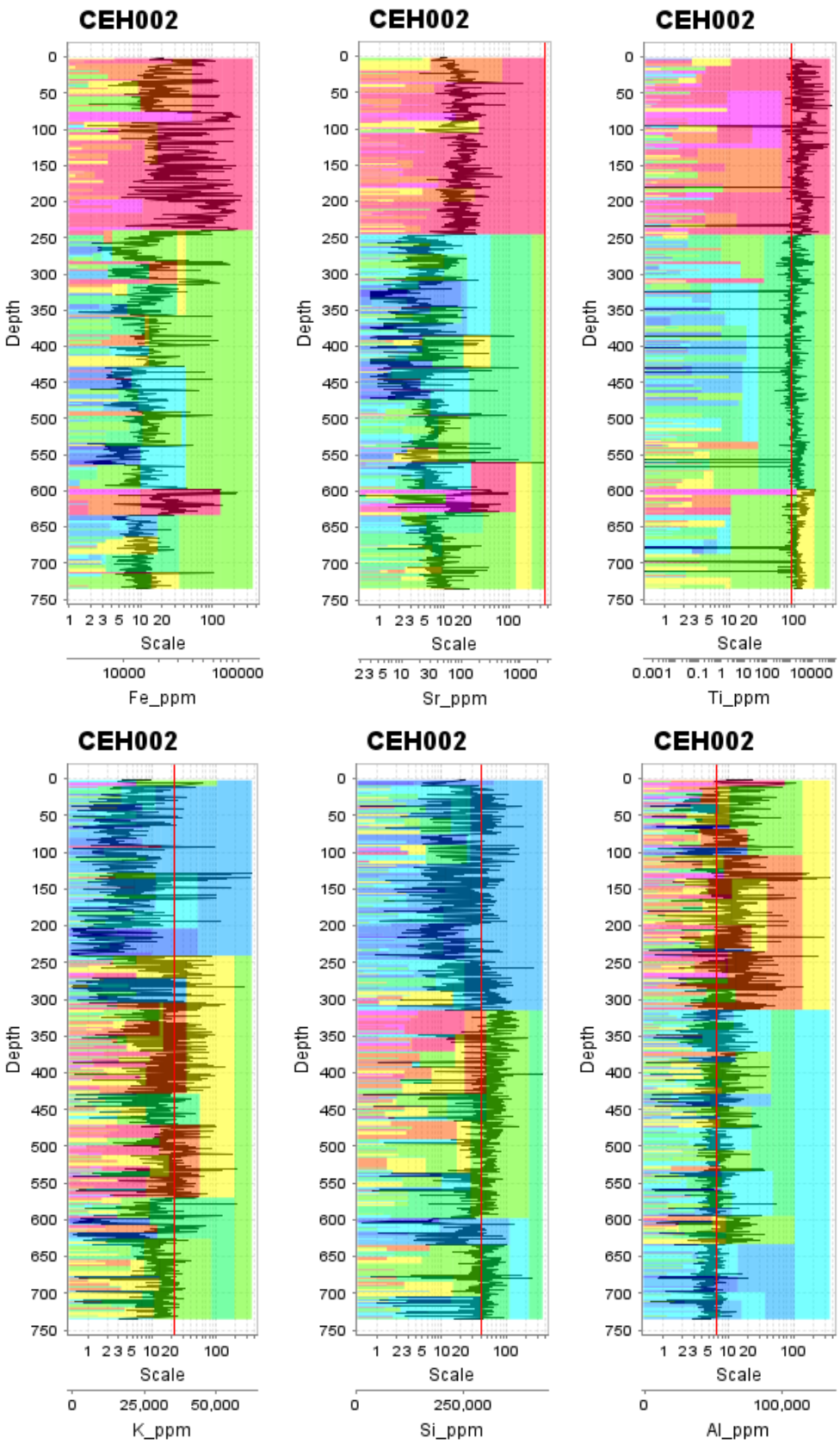


*Figure 25: Downhole Wavelet Tessellations of select elements demonstrating major stratigraphic boundaries at 249m (Western Henty Fault) (Fe, Sr, Ti, K, Al and 305m (start of Mount Julia Rhyolite unit (Si, Al, K).*

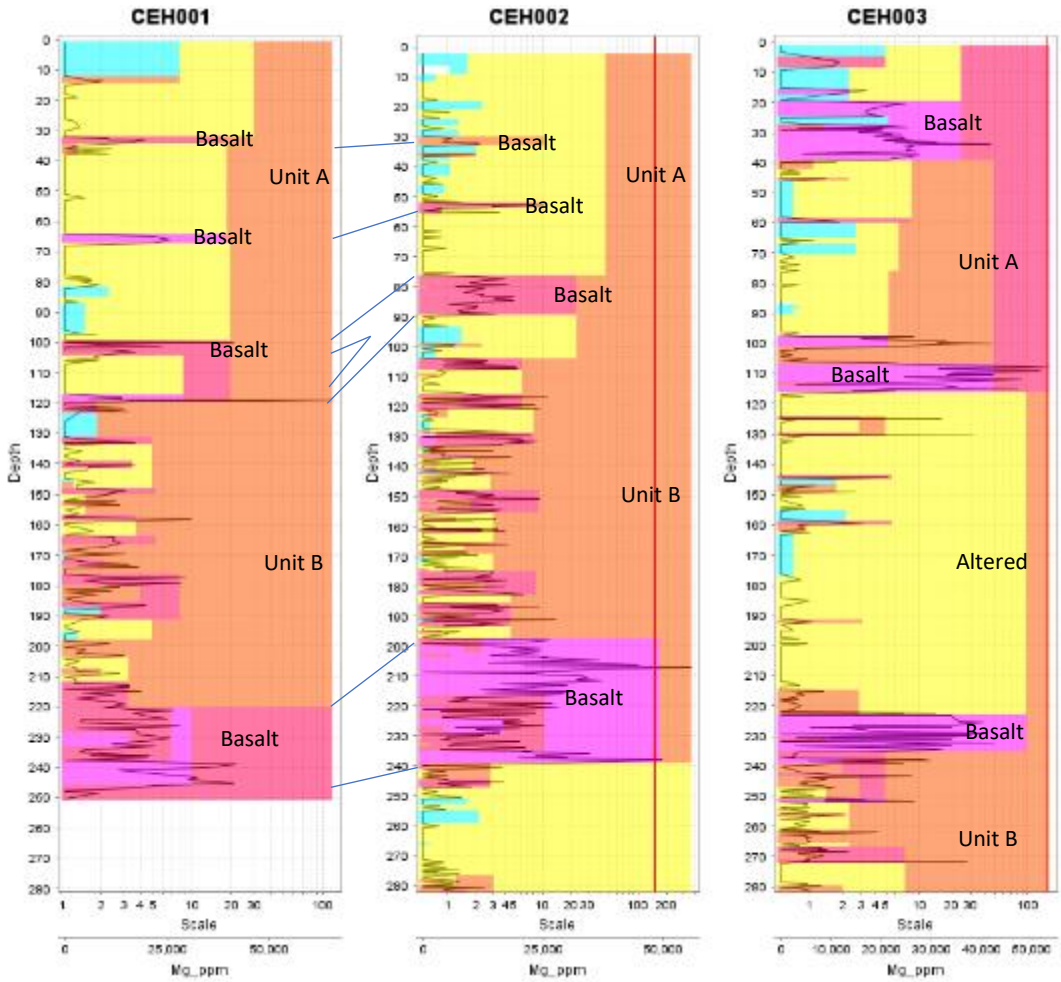


*Figure 26: Downhole Wavelet Tessellation plots for Mg in Holes CEH001, 002 & 003 showing correlations between similar mafic units in CEH001 & 002 (pink units), and other dacitic lithologies.*

Beyond these observations, there are many smaller scale variances in elemental abundance that hint at intra-lithology compositional variations, indicating sub-units of the lithology or alteration zones. Multi-element confirmation of these sub-units is not as clear as with the major inter-lithological boundaries. This analysis was conducted in ioGAS which only supports univariate tessellation analysis based on algorithms produced by CSIRO, who are currently preparing a stand-alone multi-variate tessellation program for such analysis which will be more useful for intra-lithology analysis.

An analysis across drillholes CEH001, 002 and 003 is presented in Figure 26. Data is presented with the same Y-scale in the graphs. This analysis shows that the univariate tessellation analysis can be used to interpret lithologies across multiple drillholes. In this example, the three holes present Mg content in dacitic volcaniclastics and epiclastics, and basaltic dykes of the CVC stratigraphy (to 249m depth in CEH001 & 002). The darker (red / pink) intervals represent basalt dykes. The orange, yellow and blue intervals represent correlable variation between dacitic epiclastics and volcaniclastics.

Figure 27 and Figure 28 demonstrate the application of lithochemistry to identifying discrete sub-units. The samples highlighted in these figures (all large purple circles and small green diamonds) display unique chemistry that is limited to specific visually identifiable sub-units in CEH002 & 003. These sub-units were variously logged as dacitic volcaniclastic, dacitic epiclastic and rhyolitic epiclastic.

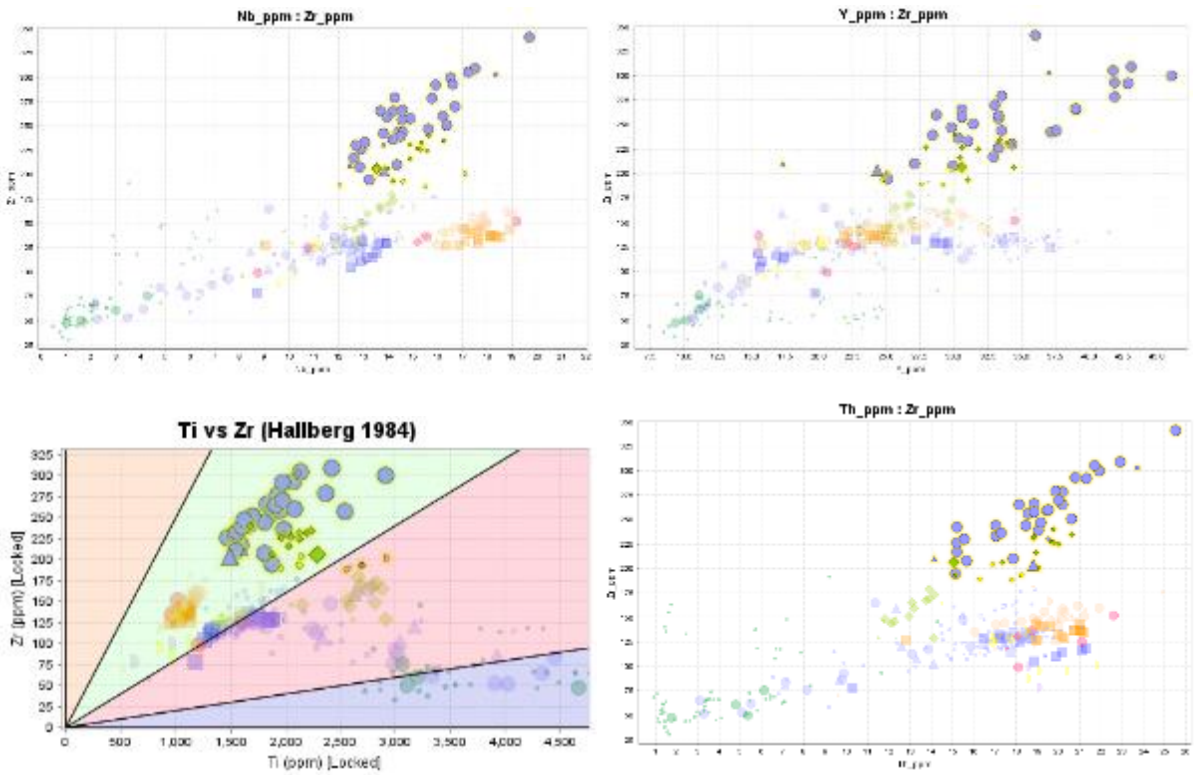


*Figure 27: X-Y plots demonstrating unique geochemistry of altered interval in CEH002 & 003 (ICPMS data). Highlighted samples represent an altered interval.*

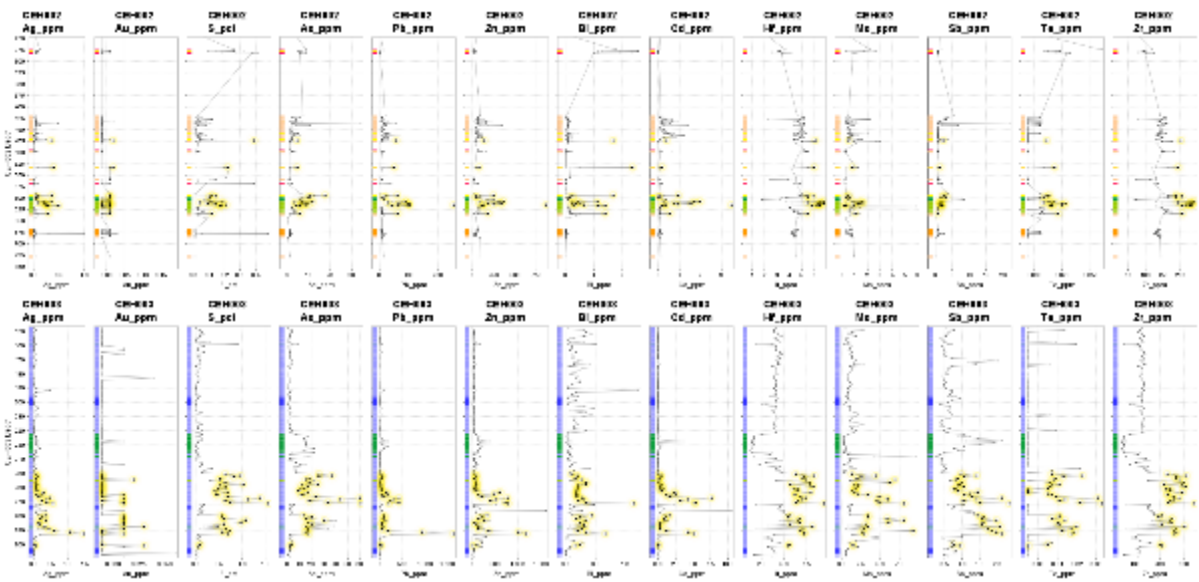

*Figure 28: Downhole plots of anomalous chemistry in CEH002 & 003 (ICPMS data). Highlighted samples represent an altered interval.*

These lithologies bracket other Late High-Mg basalt intrusive and unaltered volcaniclastic. Closer inspection of the core based on the results of geochemical analysis suggests that all of the anomalous material may represent a singular alteration or lithology. Given the similarity in pathfinder element profile of all these samples, and their presence on both the east and west side of the Henty Fault, it is

significant to determine the provenance of the material and alteration. There is evidence in core within these sub-units for movement of titanium, forming disseminated titanite, but no evidence for movement of zirconium.

These sub-units are geochemically identifiable by a number of elevated cations. The diagrams presented here primarily use relatively elevated Zr to discriminate the sub-units. Figure 27 also shows how Nb & Y can collectively be used to discriminate rhyolite from dacite, and how Th can be used to discriminate basalt.

The relevant intersection in CEH002 is described below, with the geochemically anomalous intervals highlighted in bold. The interval is bracketed by quartz phyric rhyolite:

- **593.45-597.6m; Si altered rock, logged as rhyolitic epiclastic. Altered upper contact.**
- 597.6-604.7m; Basalt, chilled intrusive margins, intensely faulted from 601.9-604.7m.
- **604.7-618.05m; Si altered rock, logged as andesitic sandstone.**
- 618.05-633.8m; Lithic volcaniclastic, interpreted as Lynchford Tuff.
- **633.8-634.55m; Si altered rock, logged as andesitic volcanic breccia. QzVn on lower contact.**

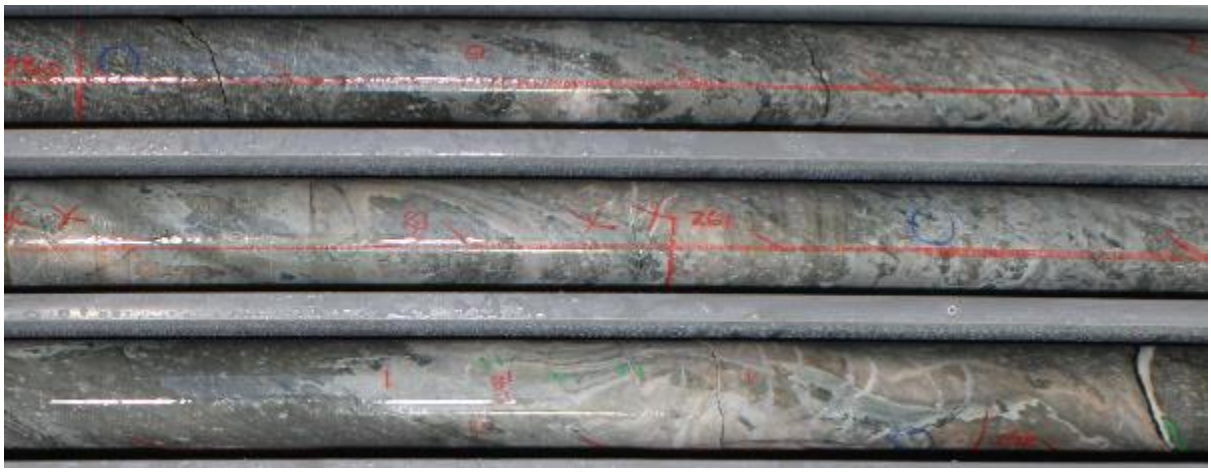

*Figure 29: Example of core from 260-262m in CEH003 demonstrating alteration associated with chemistry outlined in Figure 27 & Figure 28. Full altered interval extends from 250-293m.*

The relevant intersection in CEH003 is described below, with the geochemically anomalous intervals highlighted in bold. The interval is bracketed by quartz phyric rhyolite:

- 250-271.5m; Si altered dacitic volcaniclastics.
- 271.5-279.5m; Hematitic alteration of volcaniclastic dacite assoc. with Qz-Chl-Cb veins.
- 279.5-292.5m; Si altered dacitic volcaniclastics and epiclastics.
- 292.5-299.5m; Dacitic epiclastics

The unit in CEH003 excludes unaltered andesite or dacite at 254.95-255.9m, and unaltered basalts at 286.5-287.1m and 287.95-289.1m. These intervals can be discriminated based on their chemistry.

The alteration in CEH003 (e.g.: Figure 29) appears to be largely preferential fluid flow along possibly chemically receptive finer grained sedimentary bands within an epiclastic to volcaniclastic dacitic pile.

Alteration in CEH002 is within a more homogenous fine-grained unit and is more evenly distributed within that unit.

### 3.2.2. Pathfinder Chemistry

There were no intercepts of economic interest in the three holes completed in this program.

There is evidence of a fluid pathway observed in CEH002 and CEH003 (Figure 28) with anomalous elevated (ICPMS) results for Ag-Au-S-As-Pb-Zn-Bi-Cd-Hf-Mo-Sb-Te relative to other sampled intervals. Although the results are elevated, they indicate a low tenor pathfinder footprint and not results of immediate economic interest.

There is no significant indication of an IRG character fluid pathway in pXRF data in the vicinity of the eastern side of the Henty Fault. Typically geochemical evidence of these fluids is found within 50m east of the Henty Fault. This is most likely due to the low tenor of geochemical anomalism this far from the Henty orebody.

The study of pXRF pathfinder data was the primary objective in this part of the program to determine how effective the technique would for defining low tenor footprints of mineral fluid pathways away from primary mineral trap-sites. Geochemical comparison is made with the limited ICPMS low-level detection data also collected in this program. The majority of the anomalism detected in ICPMS data was not identified by pXRF analysis, though there are certain spot-highs identified in the pXRF data that would indicate follow-up ICPMS sampling may be productive. It is concluded the pXRF is of limited use for distal pathfinder footprint analysis but may be used with caution as a preliminary guide to assess prospectivity.

There is one zone of stronger multi-element anomalism (pXRF) identified between 435m to 435.5m with coincident Au-Ag-As-Sb-Te-Hg-Cu-Pb-Zn associated with thin (<2cm) veins (potentially Devonian) with polymetallic sulphide mineralisation logged in core. The veins are contained within a broad intense sericite (possibly muscovite) – silica alteration zone within a broad high ductile strain structural zone, representing a probably post-Cambrian proto-shear and fluid pathway.

The data sets available in this study were not ideally suitable for comparison of pathfinder element anomalies and elemental associations due to low abundance of relevant elements. The pathfinder elements are also generally at a tenor that is at or generally below the pXRF level of detection. However, it was notable that there was a broad very weakly elevated As-Te-S-Zn-Ag-Sb anomaly within the area between 227m to 293m in CEH003, and this was generally reflected in both ICPMS and pXRF data sets. The results are more erratic in the pXRF data as the tenor is near instrument detection limits. There is also a Cu anomaly in ICPMS data in CEH003 that is not reflected in the pXRF data, however this appears to represent a lithological feature (mafic dyke).

Several key aspects relating to pathfinder chemistry are described below and displayed in Figure 30. It should be noted that Au readings of <~10ppm may be spurious due to the difficulty associated with reading Au on pXRF.

**Henty Fault**

In CEH002, the Henty Fault is highlighted by anomalous Mg, S associated with pyrite, weakly elevated W, and detectable Au. The most geochemically anomalous interval is 280m to 287m which contains significant late fuchsite alteration.

**Cu distribution**

The area including the Henty Fault and downhole to 480m is anomalously and consistently depleted in Cu. The zone comprises rhyolite and felsic derivatives, but there is otherwise no clear lithological or lithochemical distinction between the Cu depleted rhyolite or other rhyolite further downhole. The end of the Cu depleted zone is coincident though with the end of the intensely sericite altered high strain structural zone described in Section 3.1.4, although the intense alteration is not consistent over the length of the low Cu zone.

No clear explanation is evident for the apparent Cu depletion. We hypothesize that part of the explanation is mobility of Cu, and therefore possibly other elements, in zones of intense alteration. The alteration is interpreted to be Devonian as the strain fabric in this area is approximately NW oriented, however further geochronological evidence is required to validate this interpretation.

Figure 32 demonstrates a correlation between S & Fe with As in samples with elevated S, Fe & As. This result indicates there is an association between As and pyrite. Other metal associations with pyrite are indicated by correlations of S with Hg, Ag & Zn.

Plotting Fe against S (Figure 32) shows two distinct correlable populations, indicating multiple species of sulphide may be present. Significant populations of severally high Fe & S are present. The Fe is potentially lithological in nature, however there is no explanation for the high S without Fe at this time.

**Te distribution**

In this study, there were a significant number of Te results in pXRF data delivered consistently in the range 28 to 50ppm. The wide and unconstrained nature of the Te results indicates that these results are spurious and may reflect mineral reflectance wavelength reading error.

| **Bi distribution** | **As distribution** |
|---|---|
| Bi is a key pathfinder for Au mineralisation at Henty. In pXRF data there is only one occurrence of Bi in CEH002 supported by other elements. | Zones of elevated As intersected in CEH002: |
| • 435.4-435.5m; Au (10ppm), Ag (15ppm), S, Cu, Pb, Zn, As, Sb, Hg<br>• 440.2m; Cu, Zn, Pb, S, As, Hg<br>• 460.9m; Au, S, Pb, Zn, As, In, Hg<br>• 560m; Au (6ppm), Ag (32ppm), Sn, S, Cu, Zn,<br>• 566.15; Au, Sn, S, As, Cr, Co, Mo, Hg<br>• 594m; As, Cu, Pb, Zn | • 345-347.5<br>• 433.1-458.6<br>• 469.85-473.7<br>• 668-678.7<br>• 678.7-679.25 |

| | |
|---|---|
| • 681.75m; As, Pb, Zn, S, Sn, Hg<br>• 713.9m; As, S, Pb, Au (6ppm), Mo<br>• 726.1m; As (60ppm), Pb, S, Au (7ppm)<br>• 731.25m elevated Bi, Pb, S, As, Cr. | |

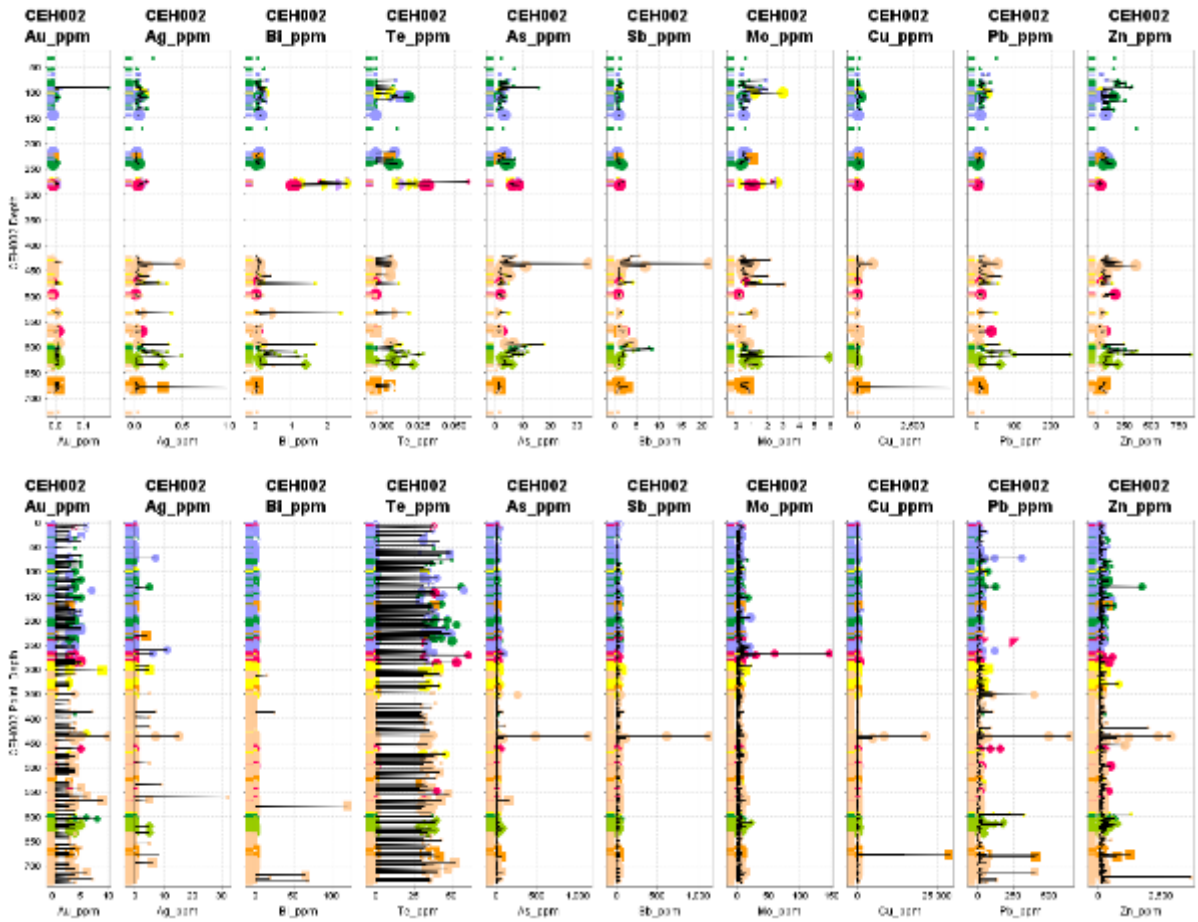


*Figure 30: Downhole plots of pathfinder elements for CEH002 using ICPMS data (top) and pXRF data (bottom).*

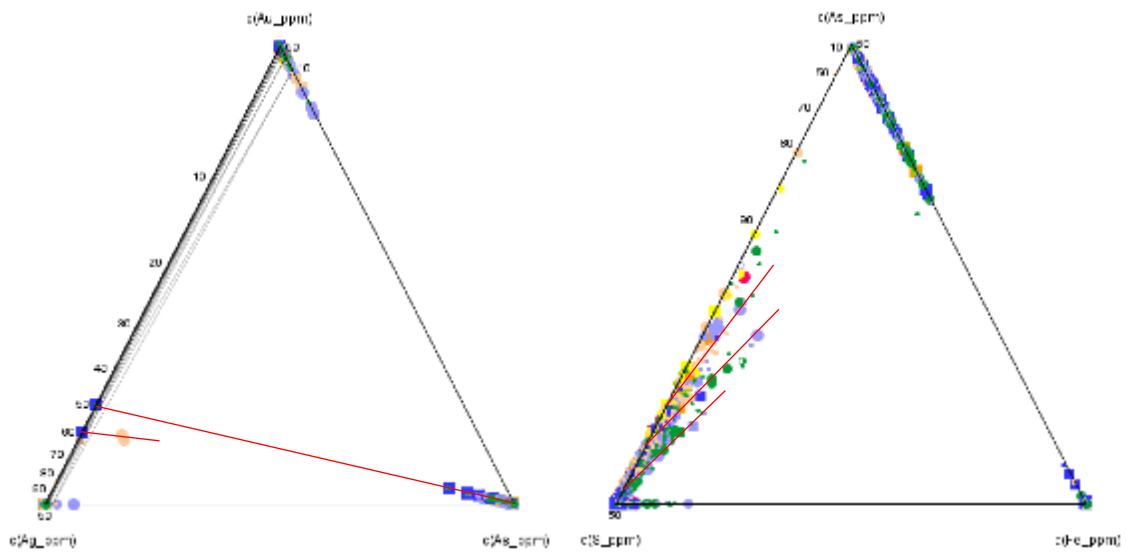

*Figure 31: Ternary analysis of pathfinder elements demonstrating Au-Ag-As metal association in a small sub-population of samples. This was found to be the most reliable metal association with gold identified in samples from this drilling program.*

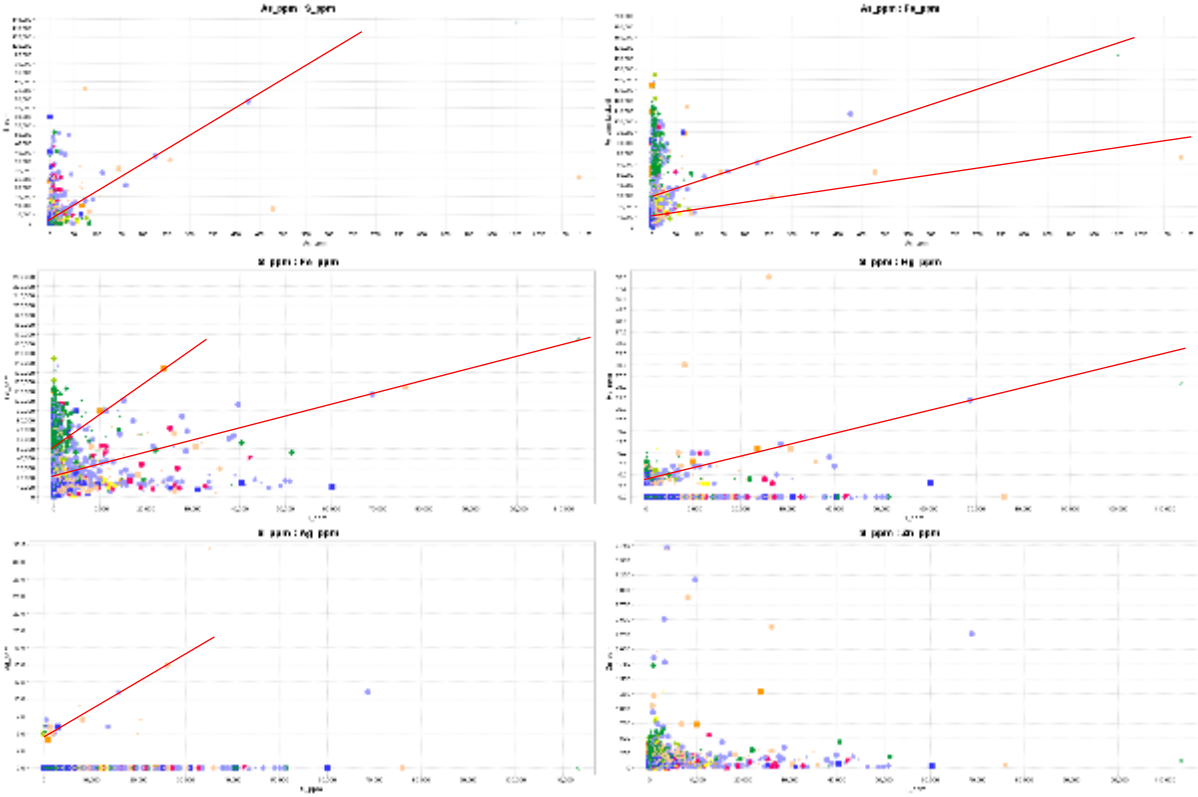

*Figure 32: Analysis of positive correlations of (left to right) S & Fe with As, and of Fe, Hg, Ag & Zn with S (ICPMS data).*

## 3.3. Magnetic Susceptibility

The majority of incidence of magnetic basalts is limited to the area west of the HFZ in the upper 130m of holes CEH001 & 002.

Other occurrences are noted in close proximity to the HFZ in CEH002 (one reading), and in the High-Mg basalt dyke intersected east of the HFZ around 600m downhole in CEH002.

The incidence of a High-Mg magnetic unaltered basalt on both the east and west sides of the HFZ indicates this basalt at minimum is of post-basinal closure age.

Five of the basaltic units represented in CEH001 west of the HFZ have relatively high magnetic susceptibility. These units are located between 10m and 130m depth. There are three discrete clusters of Ti/Zr ratios represented in the magnetic units, however interpretation based upon Al, Si, K content only differentiate two basaltic events. Two events are inferred.

Some intervals logged as dacitic sandstone are reclassified as basaltic composition and have also elevated magnetic susceptibility.

## 3.4. Spectral Analysis

Spectral analysis of samples from CEH001 & 003 demonstrates that alteration proximal to the western side of the Henty Fault is dominated by muscovite, while more distal areas are more phengitic (Figure 33, Figure 34).

Larger hypogene basalt intrusions dominantly contain iron dominated chlorite and epidote alteration and contain possible amphibole. Smaller basalts in CEH003 (unclear whether hypo or epigenetic) typically contain magnesium dominated chlorites, while smaller basalts in CEH001 typically contain Fe chlorite (Figure 33, Figure 34).

We hypothesize that the significance of the difference in chlorite alterations could potentially represent difference between hypogene or epigenetic nature of the basalt. More work is required to validate this hypothesis. Basalts with Fe chlorite alteration (in CEH003) are typically smaller in size, are also affected by white mica alteration (Figure 33, Figure 34) and appear to be oriented approximately north west in the Tabberabberan orogeny orientation (Figure 13), indicating they are likely part of the depositional stratigraphy. The larger basalt in CEH003 is interpreted to be intrusive and alteration is dominated by Mg-Fe chlorite without white mica alteration. The larger intrusive basalts in CEH001 are oriented approximately north-south roughly parallel to the Henty Fault. Carbonate is poorly represented in this analysis and the only significant carbonate intercept at 222m in CEH003 is calcite.

Logged alteration is compared to spectrally defined alteration in CEH003 in (Figure 35). Although the two data sets are not entirely consistent, they both demonstrate a significant change in alteration domain above and below the significant mafic dyke centred on 230m depth, with hotter phengitic and silicic alteration up-hole of the dyke. Alteration and lithology are more erratic below this depth.

The larger Mg-Fe chloritic basalt (which is not altered by white mica) centred at 230m depth is logged as weak sericite alteration (again suggesting a relatively unaltered late intrusive nature), while the smaller Mg-Fe chloritic basalt (which is also moderately phengite altered) is logged as being strongly chlorite altered. The dominantly phengitic alteration in the core is logged as weak to strong albite-silica alteration, while the lower wavelength mica (muscovite-phengite) is logged as strong sericite alteration.

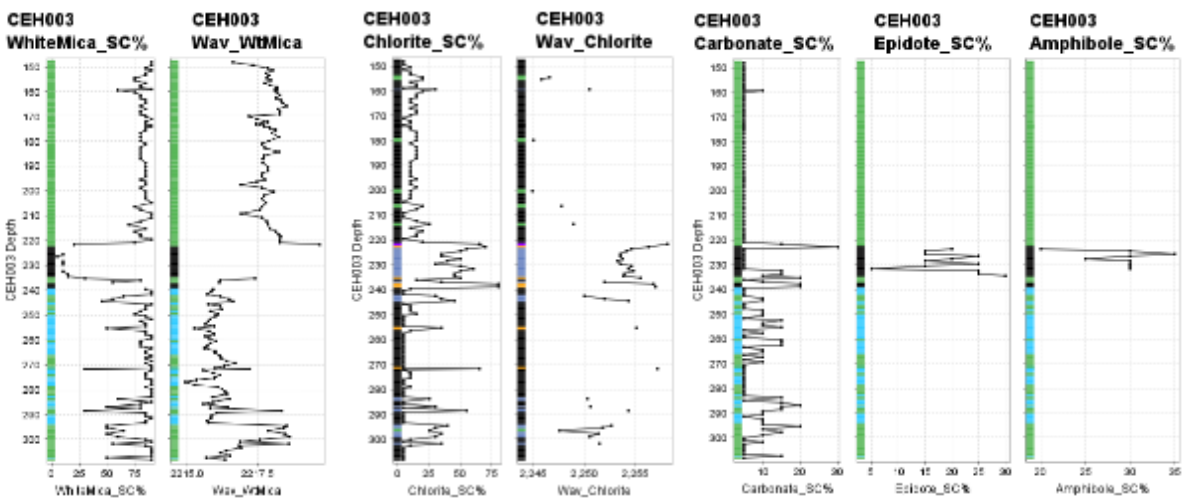


*Figure 33: Spectral analysis of CEH003 samples. Mica diagram coloured by mineral type (mica diagram; green = phengite, blue = muscovite-phengite), (chlorite diagram; pink = FeChl, orange = FeMgChl, green = MgChl, blue = MgFeChl).*

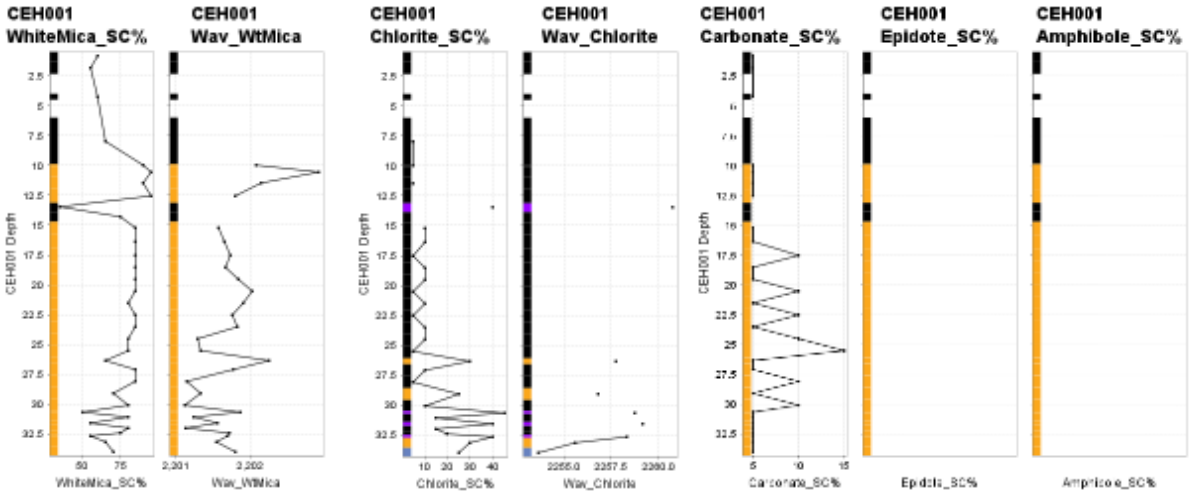


*Figure 34: Spectral analysis of CEH001 samples. Mica diagram coloured by mineral type (mica diagram; orange = muscovite), (chlorite diagram; pink = FeChl, orange = FeMgChl, green = MgChl, blue = MgFeChl).*

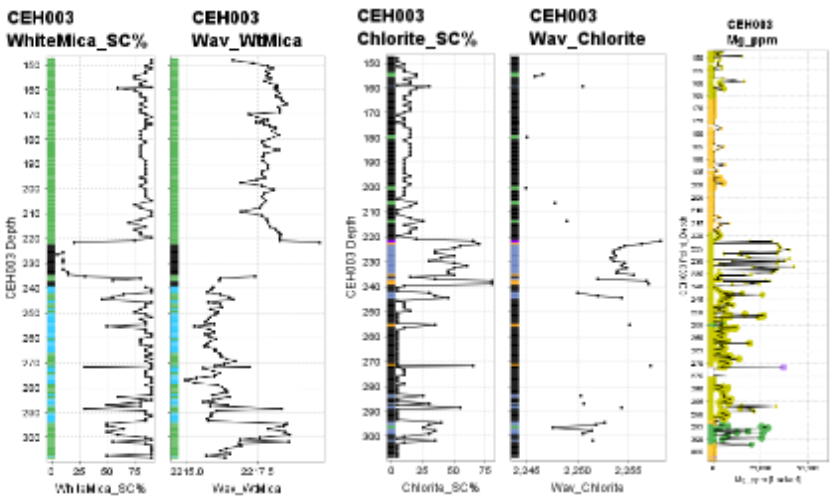


*Figure 35: Comparison of logged Vs spectrally defined alteration for CEH003. Logged dominant alteration (Mg plot) shows albite-silica (orange), sericite (light green) chlorite (dark green) and quartz (pink).*

## 3.5. Alteration Classification

Alteration discrimination and classification diagrams were trialled using ICPMS and pXRF data. A comparison was made with pXRF data which shows that the pXRF presents similar results (absent Na), but with a greater spread and lower sensitivity. Results are shown here for ICPMS data only.

Figure 36 and Figure 37 demonstrate that alteration in these holes is dominantly low intensity, tending away from alkaline towards muscovitic or sericitic alteration and towards adularia in the most intensely altered rhyolitic intervals. Some basaltic and dacitic samples are trending towards chloritic composition. There is minimal acidic alteration evident, with only a small number of silica altered samples trending towards advanced argillic alteration (Al-K-Mg Ternary Plot, Figure 36).

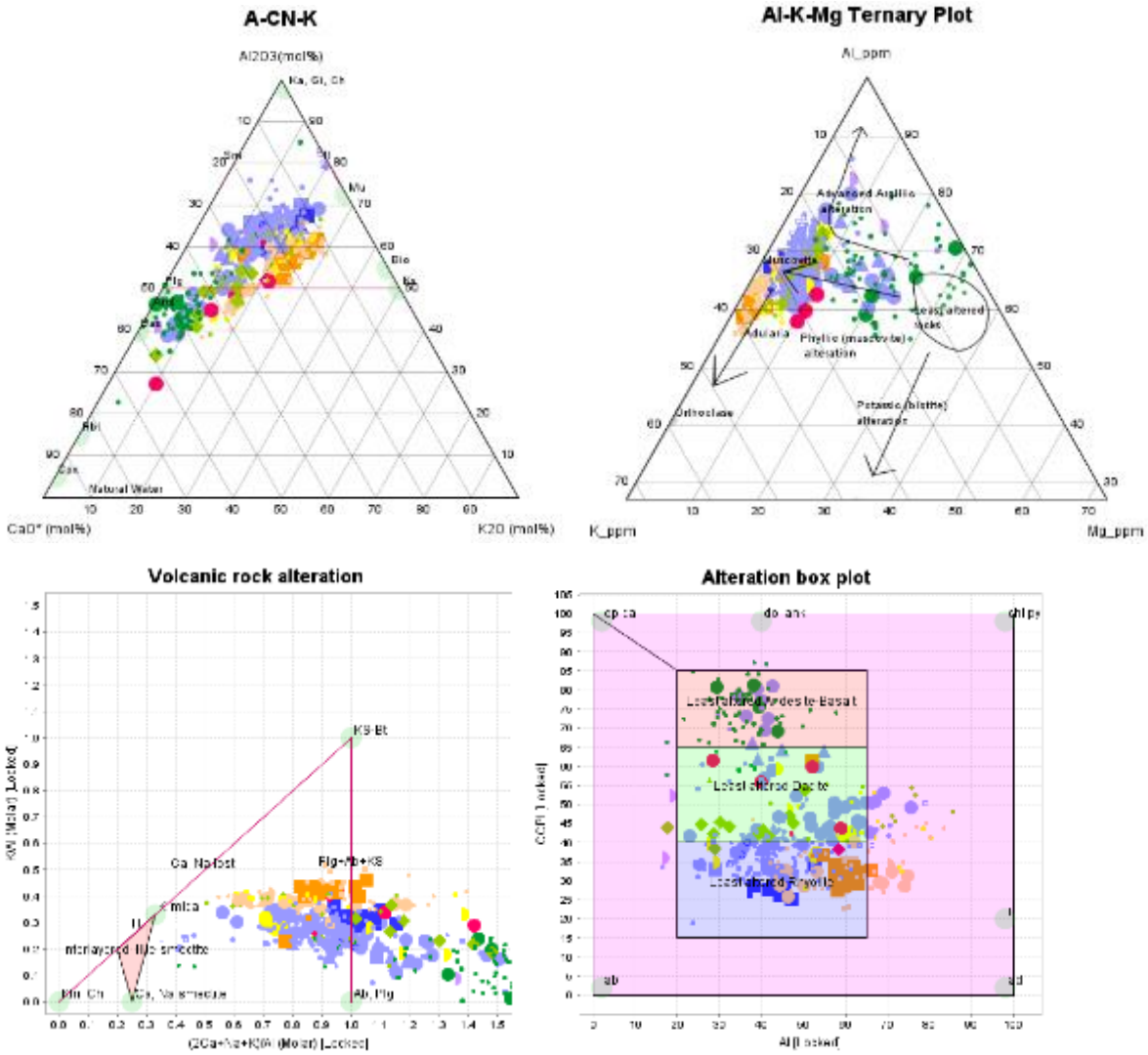


*Figure 36: Various alteration discrimination plots for determining trends in alteration style and intensity.*

### 3.5.1. Alteration Indices

Alteration indices are useful for objectively quantifying alteration intensity for mineral creation and destruction. Alteration indices have values that generally increase towards the deposit on a district and (or) deposit scale, depending on context of the alteration and proto-lithology. Five alteration indices are considered using ICPMS data for the three EDGI holes. Most of these indices utilise Na which is not directly measured by pXRF (although a proxy can be calculated). Consideration of alteration indices using pXRF data are therefore limited to the Muscovite Alteration Index (MSI) which does not require Na.

The five alteration indices considered here are:

- ISER – Sericite Index; Based on the GER of K2O and Na2O sensitive to sericite participation.
- AI – Ishikawa Alteration Index; Mg-Ca-K based alteration index, also known as the Hashimoto Index. Developed for vectoring in alteration of Kuroko style epithermal deposits.

- CCPI – Chlorite Carbonate Pyrite Index; Uses FeO (total) or Fe2O3 (total) aliased to FeO or Fe2O3. Developed for discriminating alteration zonation in epithermal deposits.
- MSI – Muscovite Saturation Index; Defines intensity of alteration and zonation which is related to gold concentration in Archean Lode deposits.
- ACNK Index; Measures relative proportion of Al against Na+Ca+K which represents the destruction of minerals, typically feldspars, throughout alteration assemblages associates with VMS deposits.

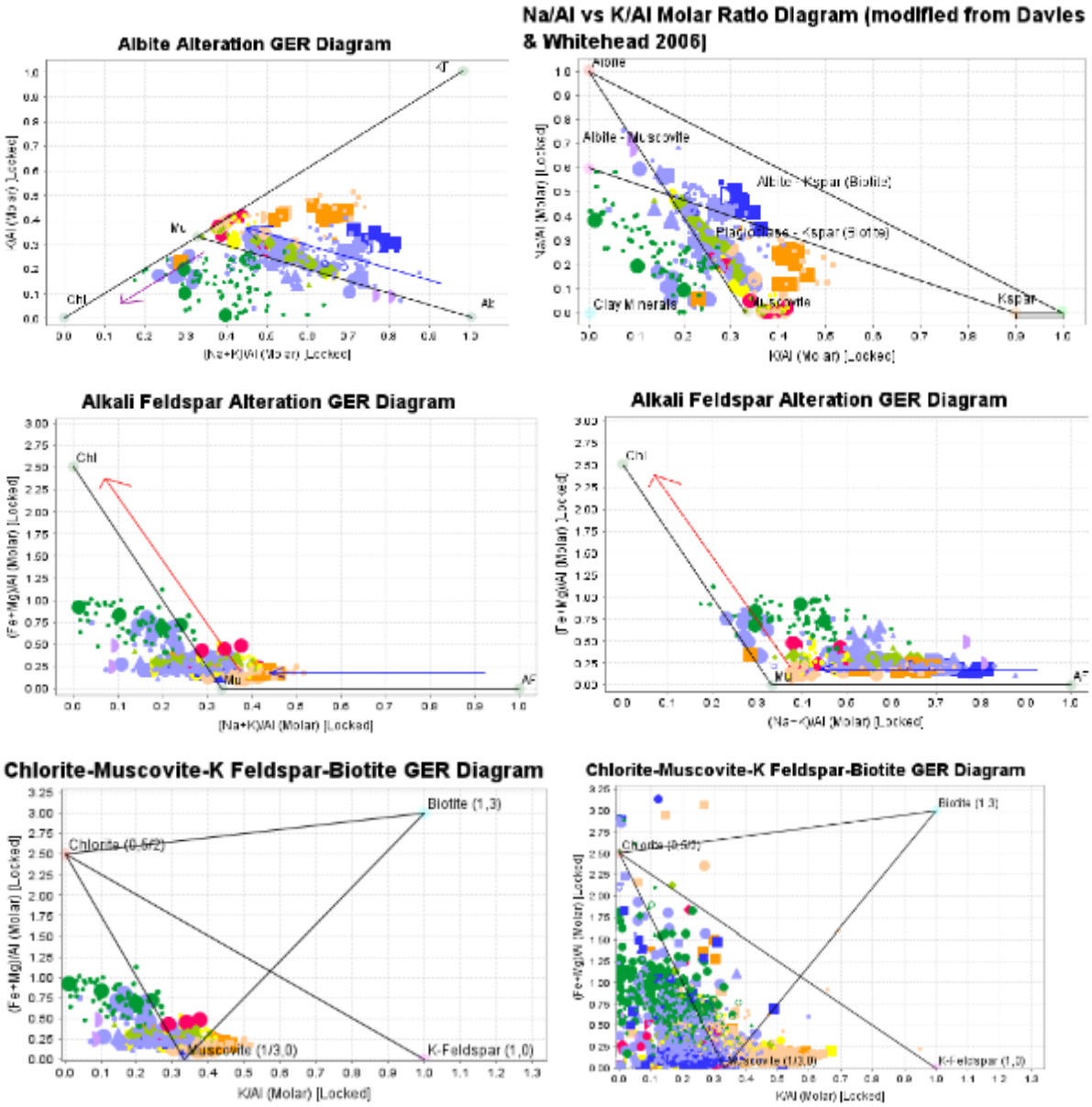


*Figure 37: Select alteration characterisation plots for analysing trends in alteration.*

Assessment and interpretation of results are provided herein, however these it is to be noted that these interpretations are not presented by a Geochemist. Further work on this data will involve assessment by a Consulting Geochemist.

#### 3.5.1.1. Assessment of Alteration Indices (ICPMS data)

The high tenor AI response down to 15m in CEH001 and elevated response for the same interval in ACNK reflect oxidative weathering. A coherent anomaly at 13-14m with sharply elevated CCPI and ACNK accompanied by decreased MSI reflects weathered basalt.

Basalts intrusions appear to be late in the paragenesis and minimally or not impacted by the early hydrothermal system. They are minimally to moderately impacted by more recent structural activity associated with the Henty Fault Zone and attendant sericite alteration. These basalts are reflected in the alteration indices by a decrease in tenor of the AI, MSI, ACNK and ISER responses (in order of amplitude and delta in changed response). The same units are reflected by increased response in CCPI.

Responses of different indices within the Henty Fault Zone are highly variable.

Generally, the response of samples taken in dacitic volcanics and epiclastics, and andesites, reflect higher CCPI and lower MSI and AI relative to rhyolitic volcanics and epiclastics, as would be anticipated. The ACNK response does not vary substantially between lithologies indicating there is not substantial destruction of feldspar on either side of the Henty Fault Zone.

Within the rhyolitic group rocks (CEH002) there is slight elevation of ACNK response both in heavily sericitised rhyolite between 414.5m to 474m and in interpreted ABSI (albite silica altered rock) at 668-678m indicating some level of feldspar destructive alteration. These locations also present a relatively higher tenor response in AI.

The MSI response in rhyolitic volcanics and volcaniclastics appears more erratic and does not appear to clearly reflect any specific alteration zones.

The Sericite Index (ISER) is theoretically the most significant index for assessment of Henty as sericite is a dominant peripheral alteration mineral to hot, acidic alteration events (muscovite and phengite), and sericite is also the primary alteration mineral in late alteration overprints of brittle structural zones (primarily muscovite).

The ISER however shows very little variation with depth or between holes, except for discrete locations within CEH002 & 003 where relatively Recent basalt dykes are intersected. The sampling incorporates a range of different lithologies and alteration styles and intensities. Further assessment by a Geochemist is required to explain the effective lack of response in this index.

#### 3.5.1.2. Assessment of Alteration Indices (pXRF data)

The Muscovite Alteration Index (MSI) was calculated and assessed for the pXRF data as it does not require input of Na. A direct comparison between ICPMS data and pXRF data are presented in Figure 39. The tenor of response using pXRF data is comparable to using ICPMS data. The resultant amplitude of intra-unit response variance of pXRF data is greater than for ICPMS data presumably due to the point sample nature of pXRF data, but overall the same patterns of gross variance in response identified in the ICPMS data can be identified in the pXRF data.

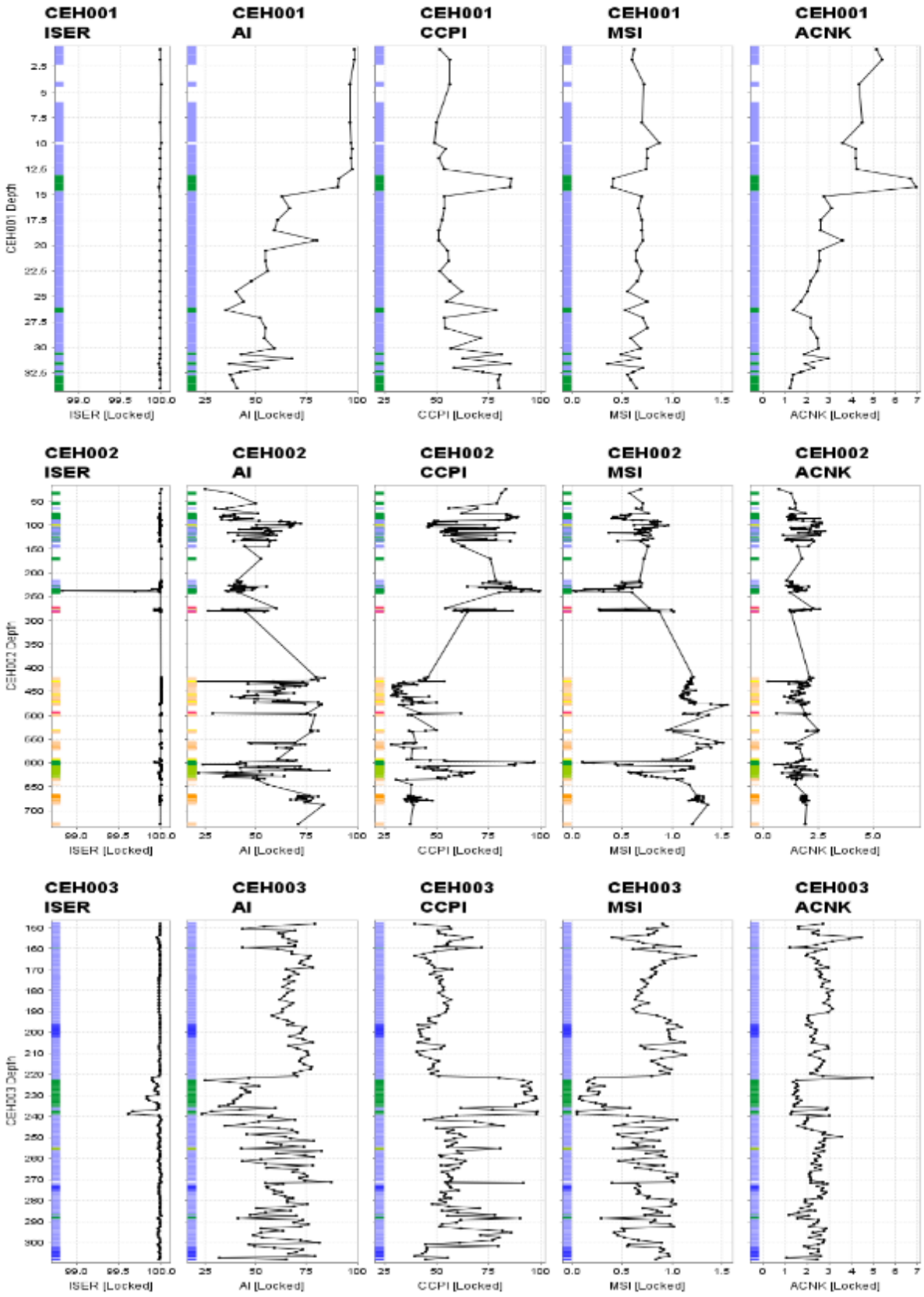


*Figure 38: Downhole plots of CEH001, 002 & 003 for exploration indices ISER, AI, CCPI, MSI & ACNK using ICPMS data (all plots). X axis is consistent between each hole for each index. Y axis is presented at different scales to provide better data resolution.*

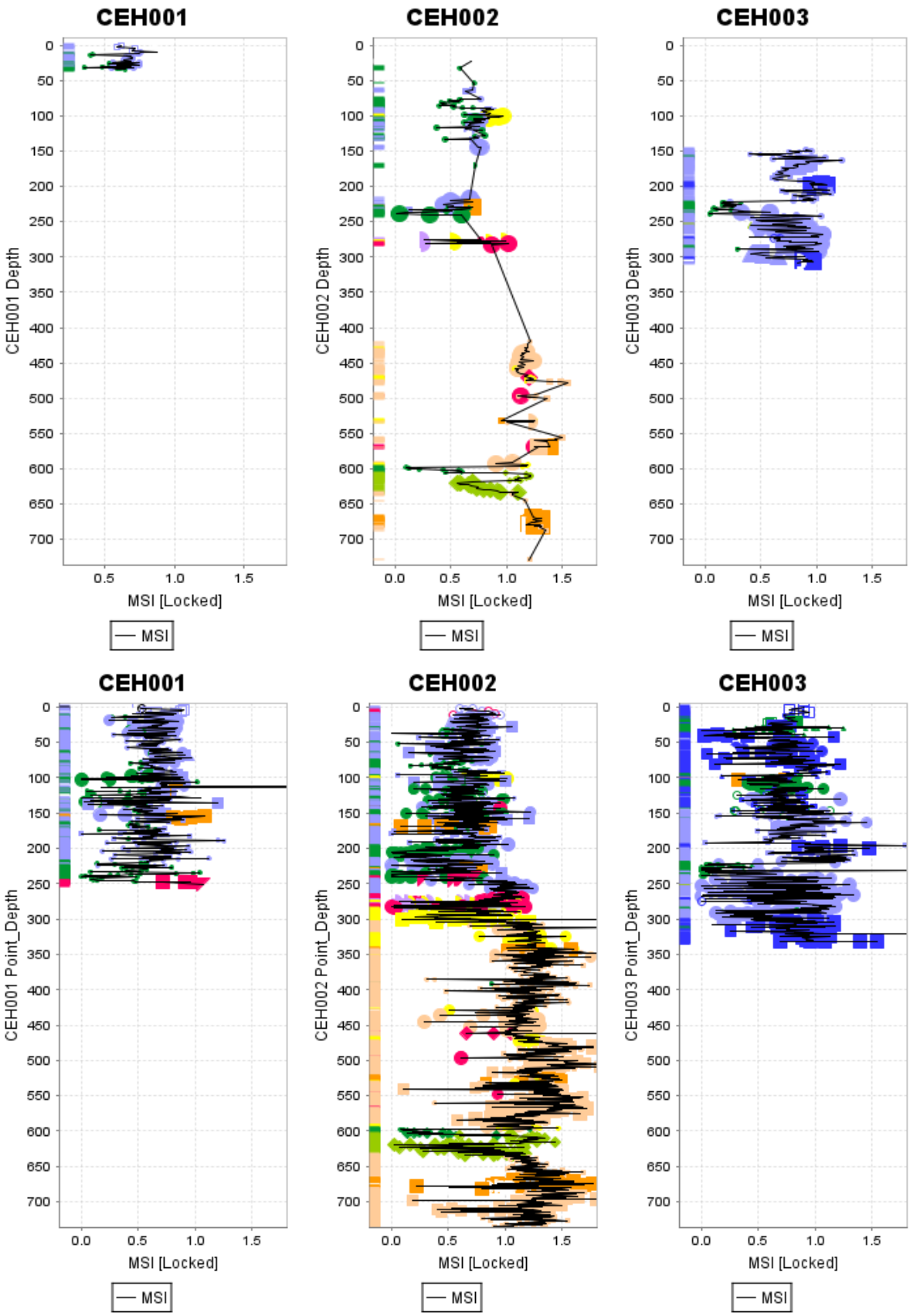


*Figure 39: Downhole plots of CEH001, 002 & 003 for MSI exploration index using ICPMS data (1st row) and pXRF data (2nd row). X-axis is consistent for all plots and the Y-axis is presented at same scale for all plots.*

## 3.6. Structural Analysis

### 3.6.1. Folded Features

Stereographic projection of all fold hinges for folds, kink bands and folded veins in CEH001 to 3 resolves a dominant ~20 to 175TN plunge with a lesser population at 60 to 335TN (Figure 40). NB: Many readings were relatively inaccurate largely due to difficulty resolving exact matches for fold closures on core.

Two principal fold orientations defined by bedding and banding are recorded within CEH drill hole data, with roughly NNE striking HFZ parallel and NNW to NW striking regional Devonian (Tabberabberan) trends. Two folds plunging ~40 to 135TN are inferred to represent the later (Figure 41). The dominant roughly HFZ strike parallel 20 to 195TN fold plunge is less evident east of the HFZ and more distal to the west in CEH003.

The HFZ parallel trends arguably split into two generations; one reflected by bedding and banding, the other being subtly different and reflected by folded veins. The various apparently folded vein types indicate formation pre-dating the last significant deformation event. Dominant folded vein plunges form two populations of 20 plunge to 175TN and a more scattered population of ~75 to 235TN, notably the latter is more common east of the HFZ. Folded vein forms are evident mostly as carbonate bearing veins with variable chlorite, quartz and minor pyrite content.

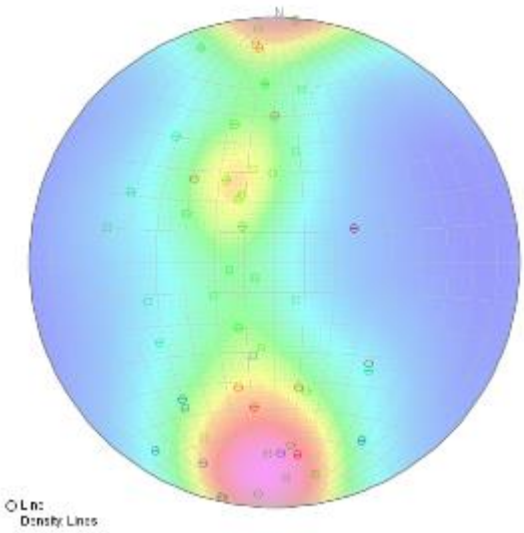


*Figure 40: All fold hinges for folds, kink bands and veins in CEH001-003 displaying dominant ~20 to 175°TN plunge with a lesser population at 60 to 335°TN.*

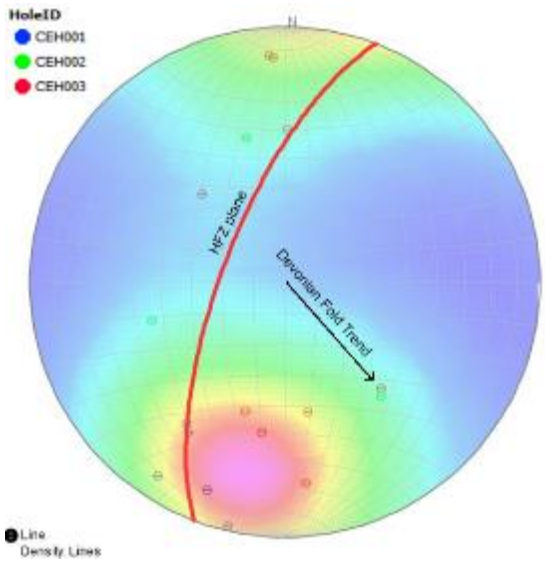


*Figure 41: Folds defined by bedding and banding showing dominant ~30 to 195°TN axial plunge.*

Kink Bands in CEH002 (Figure 43) form two weakly defined groups of plunge 60 to 325°TN and near flat plunge to 5 and 190°TN. The latter is possibly related to reverse faulting under ~WNW-ESE compression, whilst the former are possibly Tabberabberan related to reverse dextral strike slip on the HFZ, under SW-NE compression.

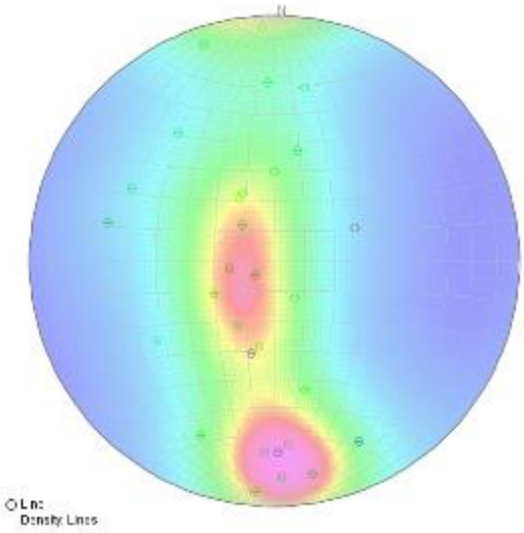


*Figure 42: Folded vein axial plane plunge and trend.*

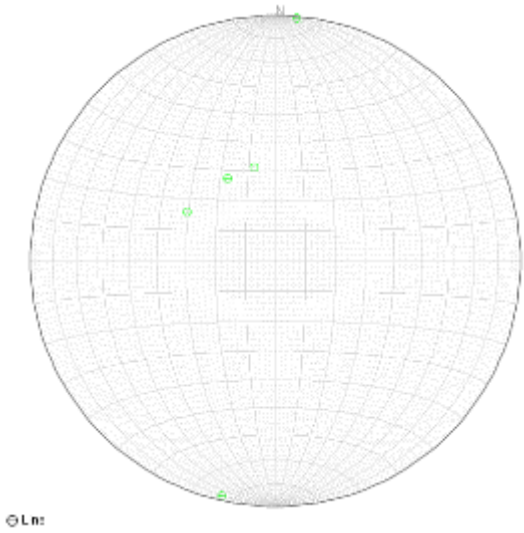


*Figure 43: Kink Bands in CEH002*

Kink Bands in CEH002 form two weakly defined groups of plunge 60 to 325°TN and near flat plunge to 5 and 190°TN. The latter is possibly related to reverse faulting under ~WNW-ESE compression, whilst the former are possibly Tabberabberan related to reverse dextral strike slip on the HFZ, under SW-NE compression.

### 3.6.2. Planar Features

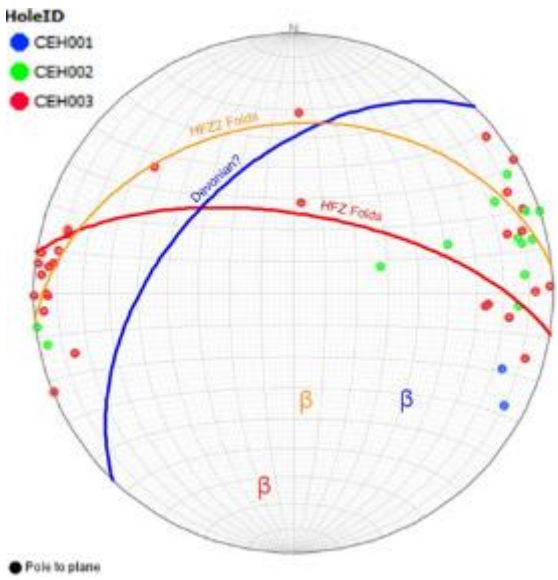


*Figure 44: Plot of all CEH poles to planes for beds and banding.*

Stereographic projection of all bedding and banding shows a scatter of mostly relatively steep SW and fewer steep NW dipping planes (Figure 44).

Figure 44 shows great circles for Devonian (blue) and two potential resolved fold plunges of 55 to 175°TN (orange) roughly matching that reflected by folded veins and 25 to 190°TN displayed by measured fold axis' from beds & bands (Figure 41).

Contacts in CEH drill holes dominantly dip steeply west (75/275°TN), particularly within CEH001 and 002 located proximal to the HFZ. This reflects a dominant ~NNE striking HFZ sub parallel orientation, whilst comparatively ~NNW strike is apparent more distal to the HFZ (Figure 45).

Basalt lavas and volcaniclastics are mostly orientated in moderate to steep west dipping, NNE striking HFZ parallel orientation, with minor influence from Devonian (NW to NNW striking Tabberaberran) trends. Basalt intrusives are similarly orientated, but a small outlier population is shallowly dipping of similar orientation to structure-related vein populations, supporting emplacement as a late-stage generation (Figure 46).

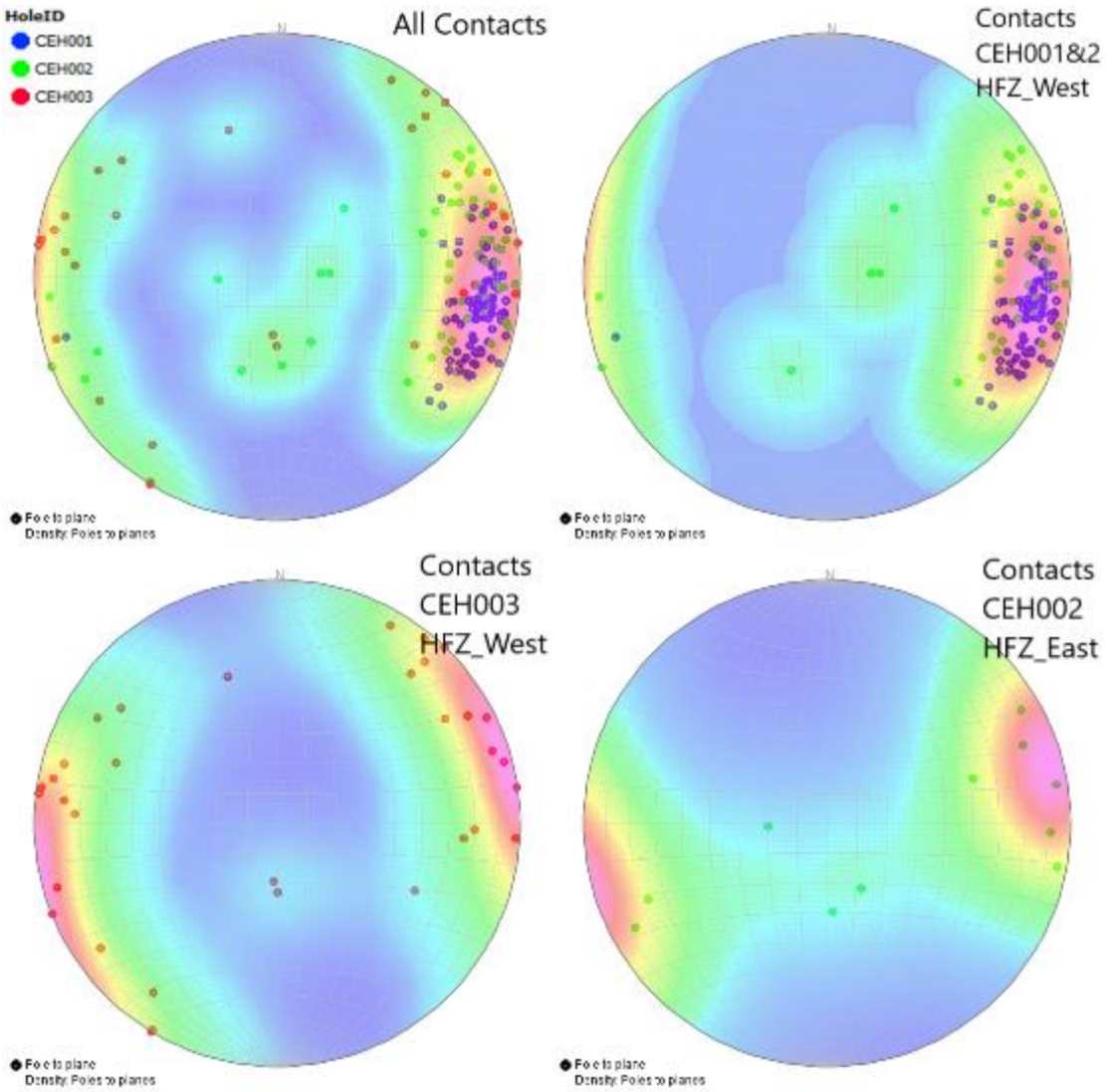


*Figure 45: Poles to planes for all Contacts with respect to HFZ East and West domains.*

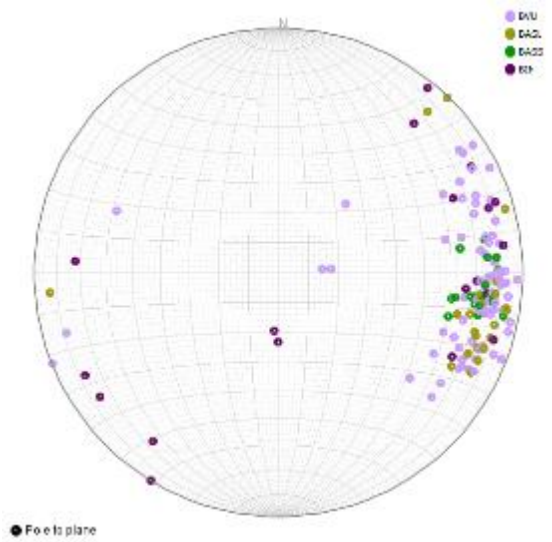

*Figure 46: Basalt Contacts (poles to planes). BVU = undifferentiated basalt, BASL = basalt lava, BASS= basaltic sandstone & BIN = basalt intrusive.*

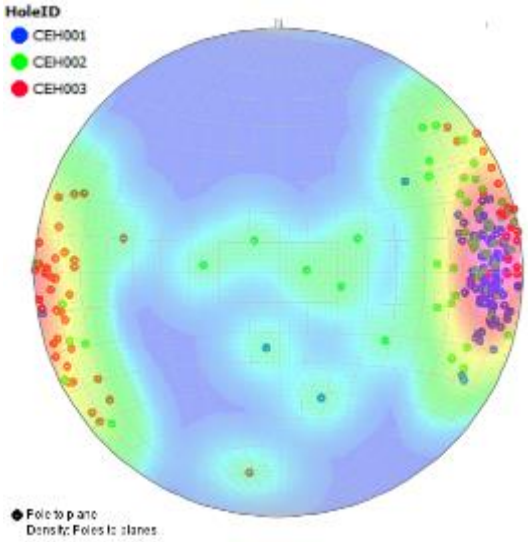


*Figure 47: Plot of poles to foliation planes.*

Figure 46 shows the dominant influence of HFZ parallel ~195°TN striking and lesser Devonian ~135°TN orientations.

Figure 47 displays mostly steep east and west dipping planes, whereas foliation in HFZ proximal basalts are almost invariably steep west dipping.

### 3.6.3. Fault Features

Analysis of key vein orientations for various mineral species identifies 3 main distributions. The Devonian NW strike trend is reflected by si, qz, sr and to a weak extent ch. A relatively flat thrust related trend is reflected by si, qz, cb, py, tan si-cb and to a lesser extent ch and sr veins. ENE to NE striking vein sets are reflected by ch, si, qz and gl. Base metals gl and cp commonly strike align to the Henty Fault (~20TN).

Reactivations on some fault planes are apparent with coincidence of some opposed shear senses. Evaluation of shear sense for all orientated faults illustrates that ~NW-SE striking (Devonian related) orientations are the dominant control, with lesser influence from NNE striking Henty Fault parallel structures.

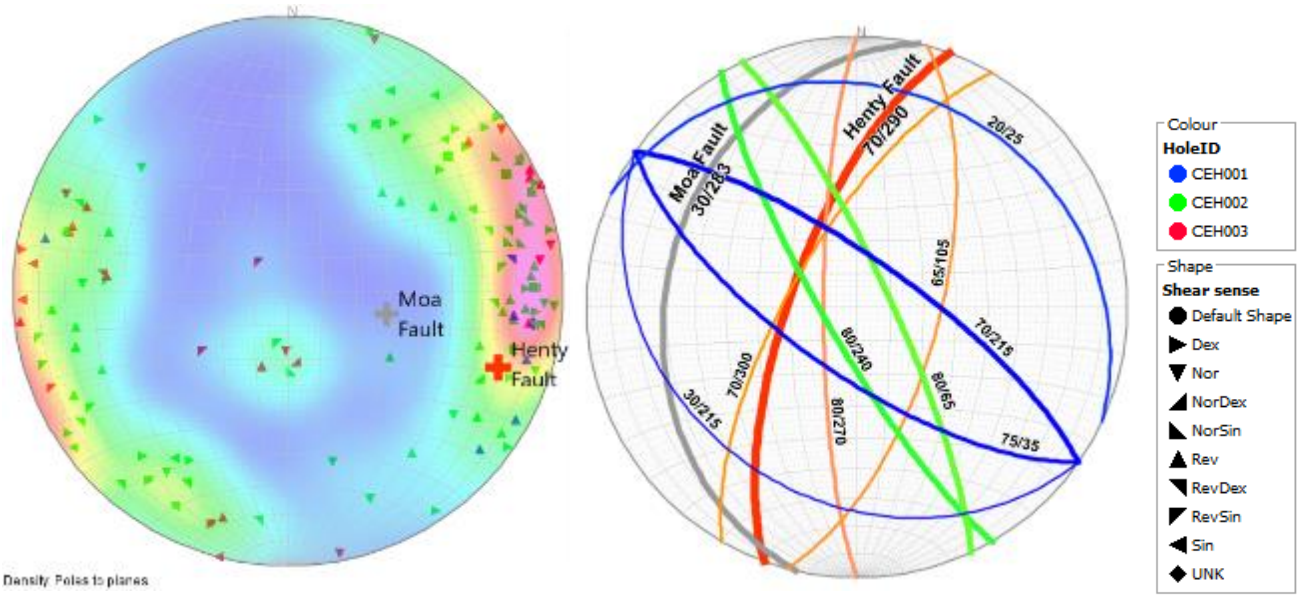


*Figure 48: Stereoplot of poles and great circles to planes for **all structural features** identified in CEH001, 002 & 003.*

*Key Fault Orientations: Planes are coloured for key fault orientations at Henty reflecting deformation stages, with line of weight indicating approximate strength / measurement density. Including Legend for all Fault movement senses and drill holes (right).*

Figure 49 illustrates that in the WHFZ domain, steep westerly dips on ~N to NNW striking orientations (black great circle) are the dominant fault control, with weak influence from shallow to moderate and steep north dipping / WNW striking faults (blue great circles), as is also weakly apparent east of the HFZ (in CEH002; grey cross = Moa Fault, Black = Henty Fault). Little Devonian NW strike influence on fault control is apparent. NNE orientated Henty Fault (70/290) -like / parallel structures are weakly expressed as reverse faults in the West of HFZ domain, whilst steep WNW dipping faults of variable

but commonly reverse apparent offsets are more common and possibly represent a conjugate set (orange great circles).

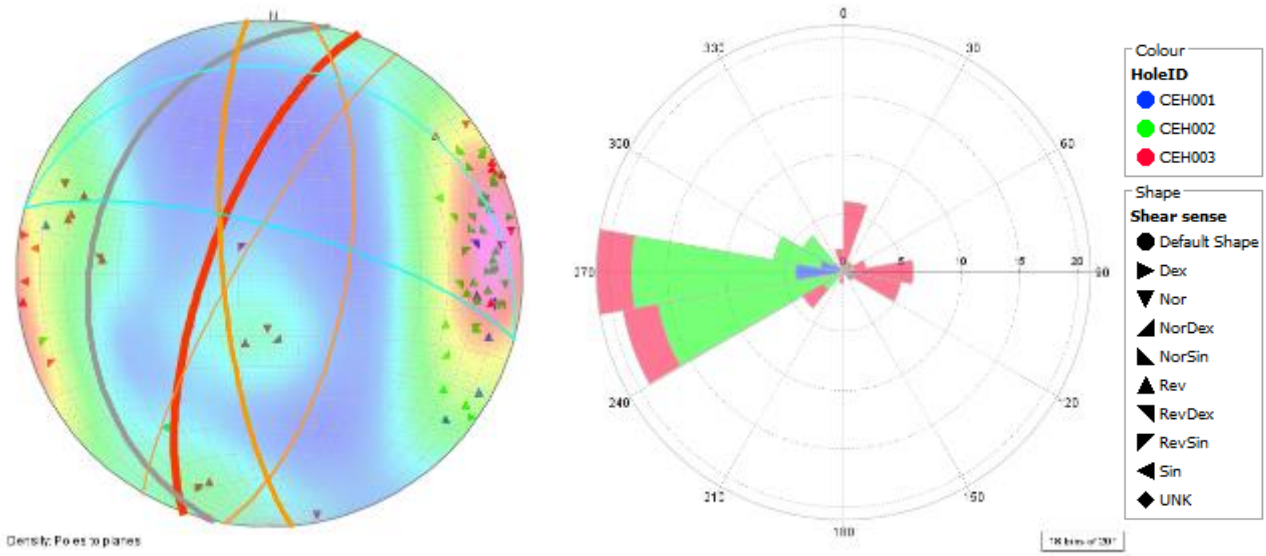


*Figure 49: Shear sense (poles to planes and Rose diagram) for all orientated fault features in the **WHFZ domain**.*

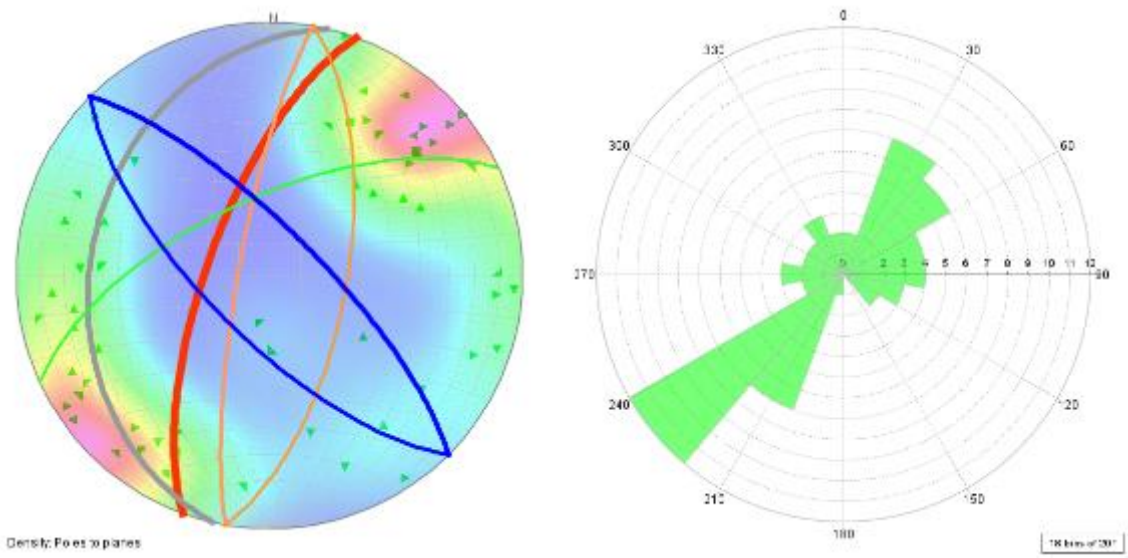

*Figure 50: Shear sense (poles to planes and Rose diagram) for all orientated fault features in the **EHFZ domain**.*

Figure 50 illustrates that that in the EHFZ domain (being hole CEH002 below the HFZ), steep east and west dips on ~NW strike, reflecting that Devonian orientations are the dominant fault control (blue great circles at 70 to 225TN and 80 to 45; grey = Moa Fault, red = Henty Fault). Henty Fault like (orange 80 to 280TN) orientations are poorly reflected, however opposed faults dipping ~65 to 100°TN are relatively more prevalent, again with very weak influence from shallow to moderate north dipping faults.

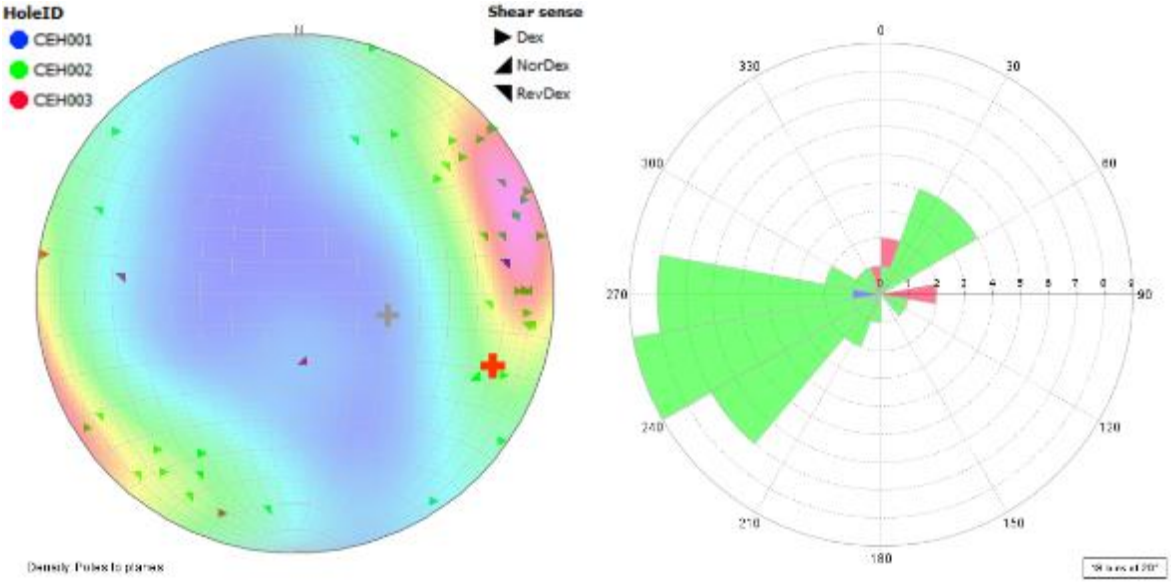


*Figure 51: Shear sense (poles to planes and Rose diagram) for all orientated **Dextral** fault features.*

All dextral faults reflect strong NW to NNW strike alignment of dominant steep WSW dip (Figure 51). The NW, likely Devonian, related strike is most evident in CEH002 (N Henty). Pole crosses are Moa Fault (grey) and Henty Fault (red).

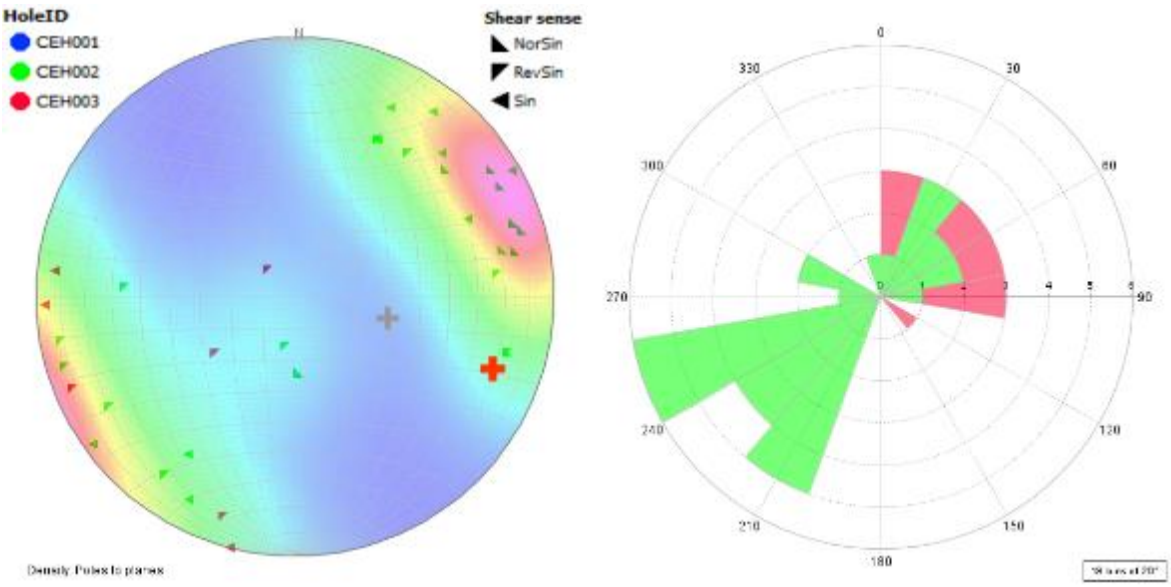


*Figure 52: Shear sense (poles to planes and Rose diagram) for all orientated **Sinistral** fault features.*

All Sinistral faults reflect strong NW strike alignment of dominant steep SW dip, but slightly rotated east in strike relative to dextral faults (Figure 52).

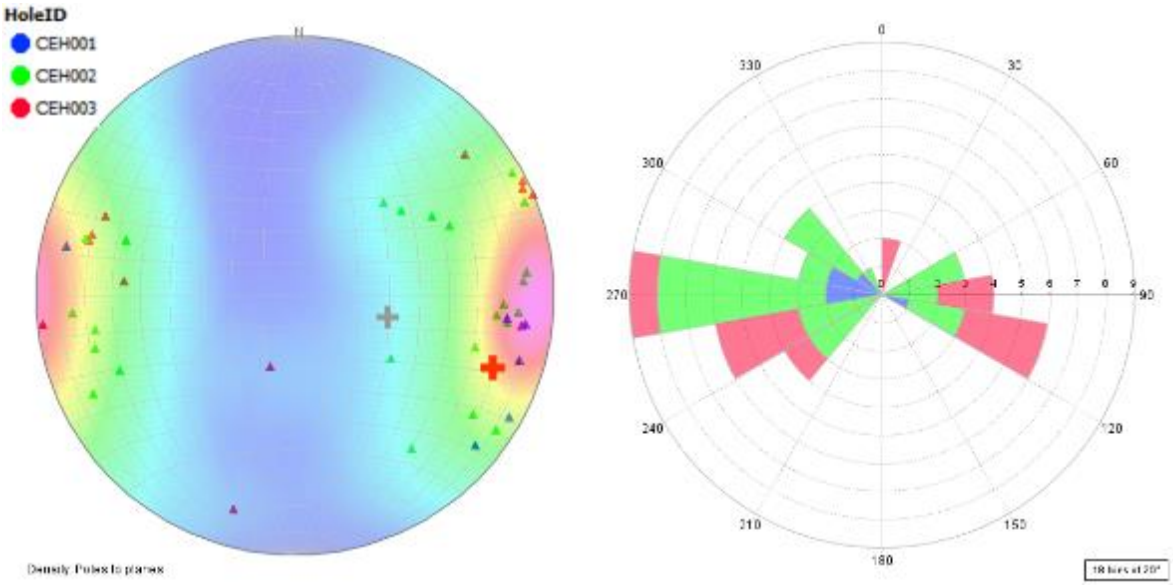


*Figure 53: Shear sense (poles to planes and Rose diagram) for all orientated **Reverse** fault features.*

All Reverse faults reflecting strong N strike alignment of dominantly steep both E & W dip. Thrust faulting reflected in an ~25/20 population (opposing 45/240) (Figure 53). A small (n=3) but tight population of reverse sinistral faults in both WHFZ and EHFZ is dips 12/145TN.

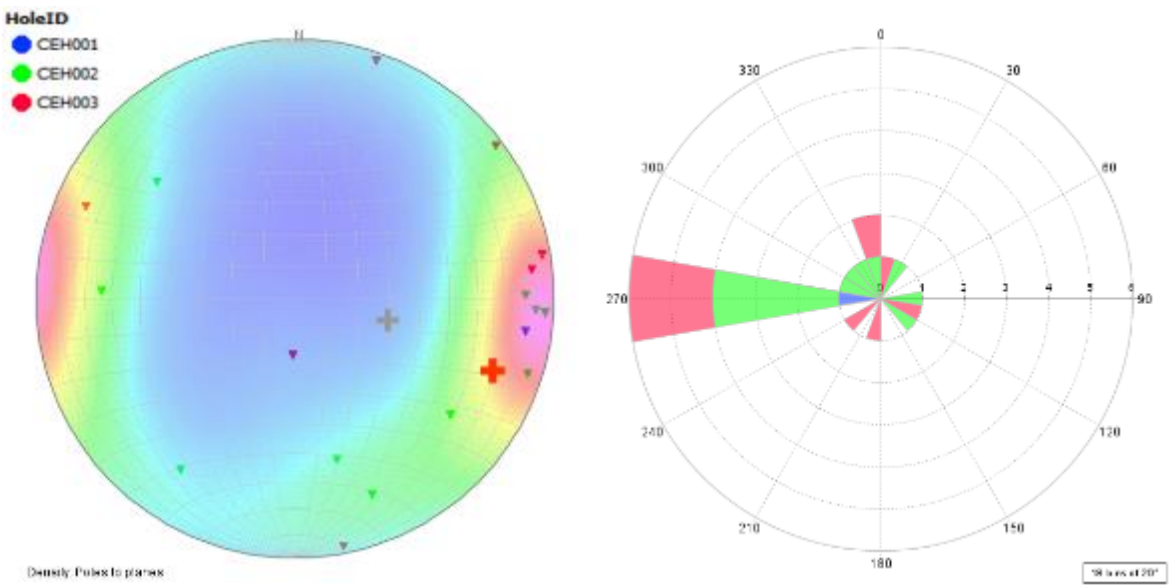


*Figure 54: Shear sense (poles to planes and Rose diagram) for all orientated **Normal** fault features.*

All Normal faults reflecting dominantly steep W dip with strong N to NNE strike alignment (Figure 54) (similar to reverse faults (Figure 53)).

Vein Features

Figure 55 illustrates key vein orientations of approximately 8/5TN, 80/265TN and a loose cluster around 75/85TN, with minor populations at 87/315TN, 85/135, 77/35 and 77/135TN.

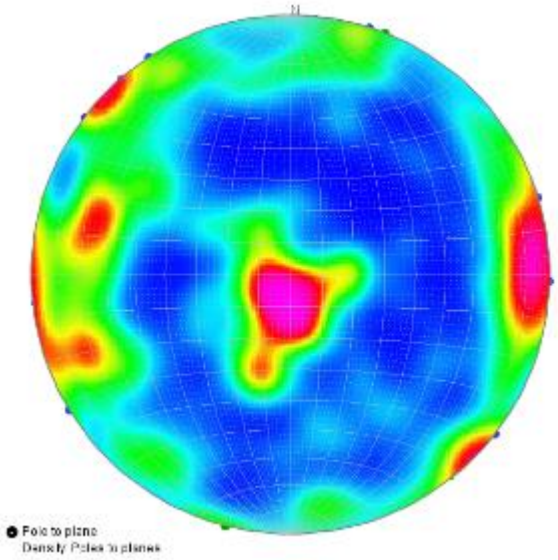


Analysis of key vein orientations for various mineral species identifies three (3) main distributions (Figure 56, Figure 57). The Devonian NNW to NW strike trend is mostly reflected by silica, quartz and sericite features. A relatively flat thrust related trend is reflected by silica, quartz, carbonate, pyrite, tan silica-carbonate and to a lesser extent albite, chlorite and sericite veins. ENE to NE striking vein sets are reflected by chlorite, silica, quartz and galena. Base metals species galena and chalcopyrite commonly align to the Henty Fault strike orientation (~20TN).

*Figure 55: Gridded density for all oriented veins (poles to planes).*

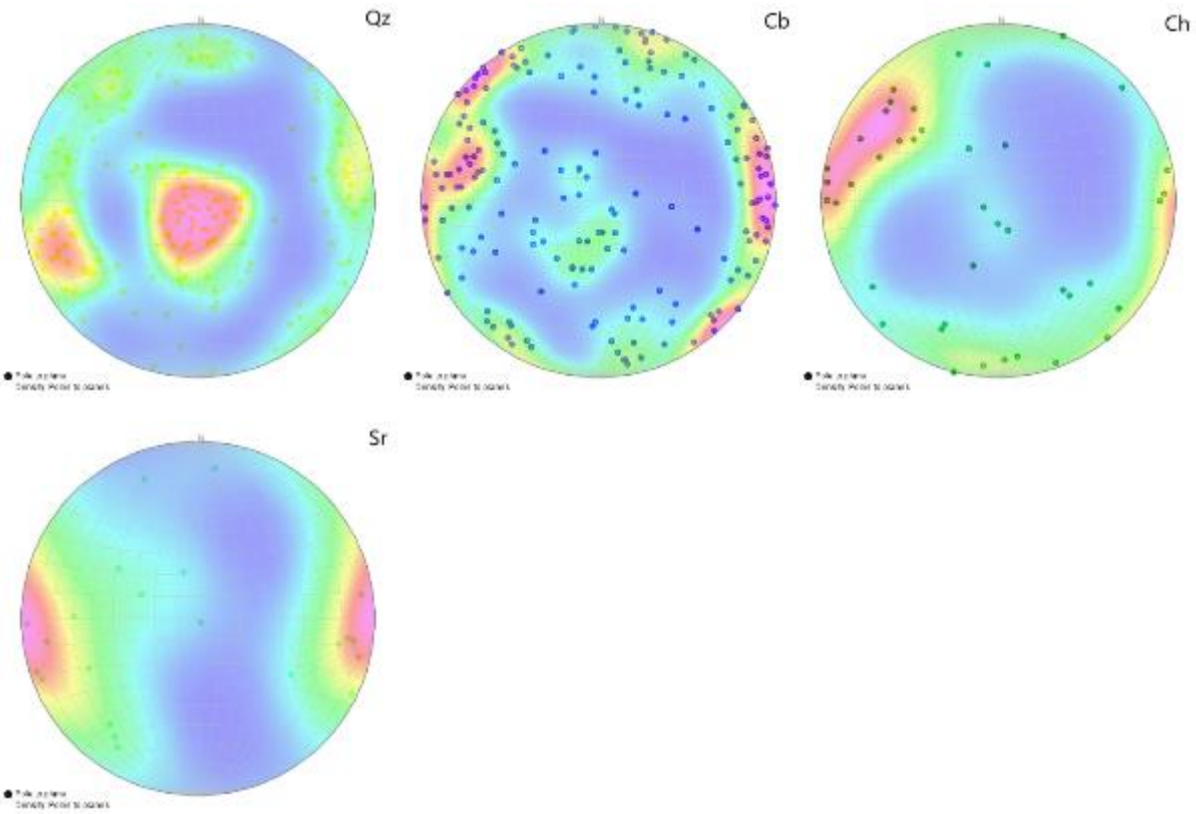


*Figure 56: Gridded density for all oriented dominant vein mineral specie (poles to planes) illustrating key vein orientations.*

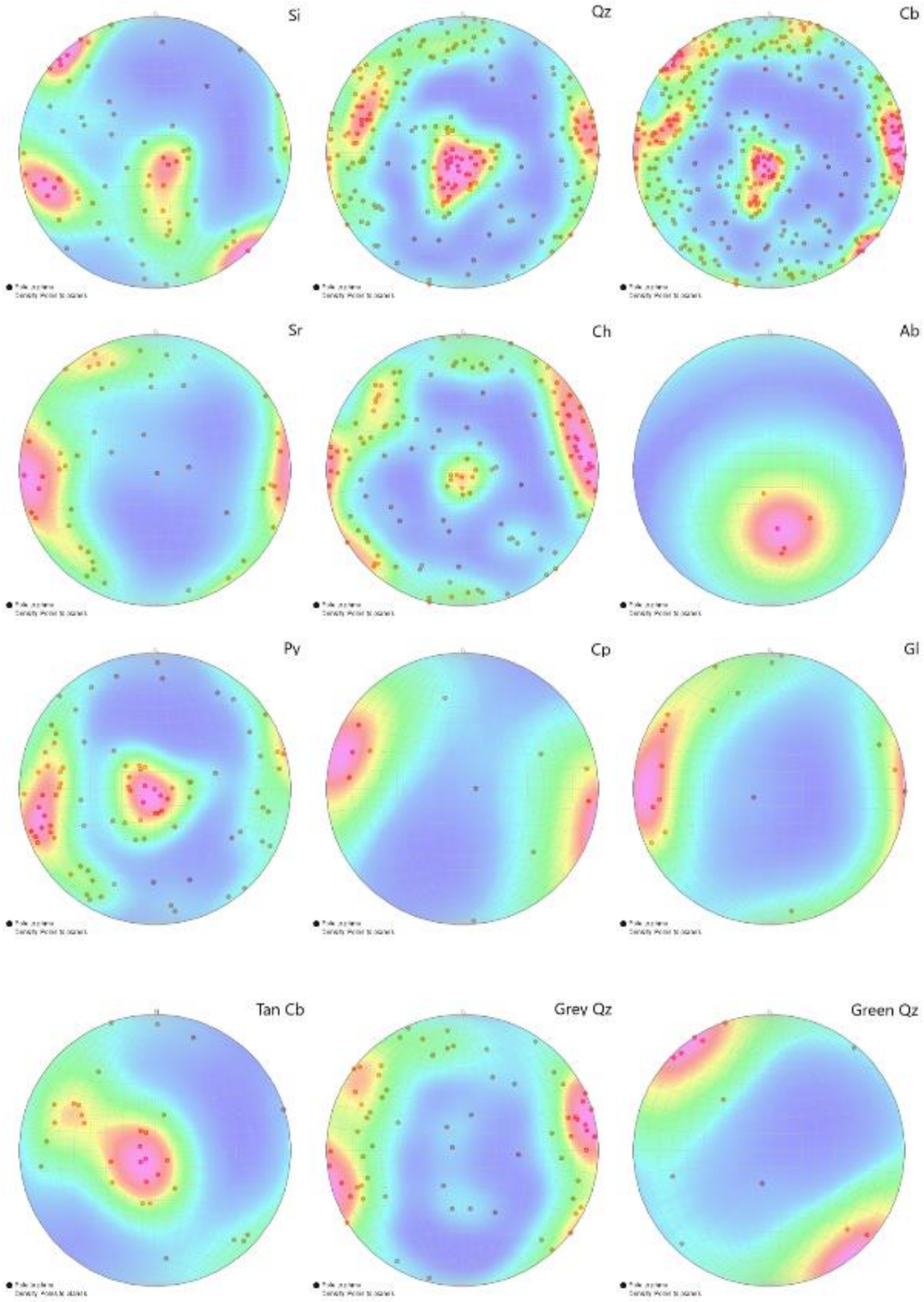
Si
Qz
Cb
Sr
Ch
Ab
Py
Cp
Gl
Tan Cb
Grey Qz
Green Qz

*Figure 57: Gridded density for all oriented veins by contained mineral specie (poles to planes) regardless of vein proportion.*

# 4. Conclusions

Economic Potential

- There were no intercepts of economic interest in the three holes completed in this program.
- There is one zone of significant multi-element anomalism between 435m to 435.5m with coincident Au-Ag-As-Sb-Te-Hg-Cu-Pb-Zn associated with thin (<2cm) veins (potentially Devonian) with polymetallic sulphide mineralisation. The veins are contained within a broad intense sericite (possibly muscovite) – silica alteration zone within a broad high ductile strain structural zone, representing a probably post-Cambrian proto-shear and fluid pathway.
- A zone of intense sericite alteration associated with a potentially Tabberabberan high strain zone in rhyolite in CEH002 is interpreted as a potential fluid pathway. The zone is apparently depleted in Cu, indicating some element mobility within the altered zone. Further work is required to validate this interpretation and develop meaningful vectors for fluid source and pathway.

**CEH001**

There are possibly three to four discrete post-depositional basaltic events represented in CEH001. At least two of these events are magnetic.

**Paragenesis**

- Basalts rich in Ni-Co-Cr located on the western side of the Henty Fault are interpreted to be the source of fluids for fuchsitic alteration within the Henty Fault and associated with late brittle shear on that structure. Spectral analysis of one of the larger basalts in CEH003 indicates the unit is not sericite altered. These observations indicate a late timing for emplacement of some of these basalts.

**Analytical Tools**

- pXRF is a suitable instrument for lithochemical analysis of drill core provided there is a sufficiently large population of data to homogenise results within a population to account for the point sample nature of each individual reading.
- pXRF is a suitable instrument for pathfinder analysis where pathfinders are present in relatively high abundance. The instrument will not generate broader coherent low level pathfinder anomalies due to the relatively higher levels of analytical detection but will likely give an indication of potential multi-element anomalism that may be followed-up with low level ICPMS analysis to discriminate fluid pathways.
- ICPMS and pXRF are producing reasonably consistent Relative levels of elemental abundance, although the Absolute elemental content levels reported is dissimilar. Consequently, ICPMS and pXRF are producing equivalent results for rock classification tools such as Ti/Zr ratios.

- **Recommendation:** Continue to use pXRF to gather broad scale lithochemical data at Henty for lithological discrimination and stratigraphic classification. Use it also for pathfinder analysis but follow-up with low level ICPMS analysis where broad low level multi-element anomalism is suspected indicating fluid pathways.

**Spectral Tools**

- TRSPEC spectral analysis of sample pulps has been an effective and cost-efficient method of obtaining broad spectral data for drilling that is superior to detailed core logging.
- Spectral analysis has provided significant detail particularly on white mica and chlorite wavelengths to discriminate variations in mineral composition which will provide thermal vectors to fluid pathways and mineralisation and support paragenetic analysis.
- **Recommendation:** Continue to obtain spectral data for regional holes and some key in-mine exploration holes when samples are submitted for ICPMS analysis. When viewing holes, take selective representative samples for either TRSPEC or Hylogger analysis to provide indication of broad alteration zonation.

**Magnetic Susceptibility**

- Magnetic susceptibility is a simple and efficient tool for lithological discrimination which has been consistently underutilised at Henty.
- **Recommendation:** Consistently capture magnetic susceptibility data with all regional and some key in-mine exploration holes.

## References

Cabanis, B & Lecolle, M 1989; 'The La/10-Y/15-Nb/8 diagram: a tool for distinguishing volcanic series and discovering crustal mixing and/or contamination, Comptes Rendus de l'Academie des Sciences, serie 2, *Science de la Terre,* vol. 309, p. 20.

Hallberg, JA 1984, 'A geochemical aid to igneous rock type identification in deeply weathered terrain', *Journal of Geochemical Exploration*, vol. 20, pp.1-8.

Halley, SW 2021; modified from: Smithies, RH & Lowrey, JR, 2022, *Eastern Goldfields greenstone geochemical barcoding project: notes to accompany 2020 data release*, Geological Survey of Western Australia, Records 2020/6.

Hastie, AR, Kerr, AC, Pearce, JA & Mitchell, SF 2007, 'Classification of altered volcanic island rocks using immobile trace elements: development of the Th-Co discrimination diagram', *Journal of Petrology*, vol. 48, no. 12, pp. 2341-2357.

Nesbitt, HW & Young, GM 1984, 'Prediction of some weathering trends of plutonic and volcanic rocks based on thermodynamic and kinetic considerations', *Geochimica et Cosmochimica Acta*, vol. 48, pp. 1523-1534.

Pearce, JA, 1996, 'A users guide to basalt discrimination diagrams', in Wyman, DA (ed) *Trace element geochemistry of volcanic rocks: applications for massive sulphide exploration*, Geological Association of Canada, Short Course Notes 12, pp. 79-113.

Rollinson, HR 1993, *Using geochemical data: evaluation, presentation, interpretation*, Routledge, London, p. 63.